Viral manipulation of a novel mechanoresponsive signaling axis disassembles processing bodies

Elizabeth L. Castle[1], Pauline Douglas[3, 5], Kristina D. Rinker[3, 4, 5], and Jennifer A. Corcoran[1, 2, 5]

[1]Department of Microbiology and Immunology, Dalhousie University, Halifax, NS, Canada
[2]Current address, Microbiology, Immunology and Infectious Diseases Department and Charbonneau Cancer Research Institute, University of Calgary, Calgary, AB, Canada.
[3]Department of Physiology and Pharmacology, University of Calgary, Calgary, AB, Canada.
[4]Department of Chemical and Petroleum Engineering and Centre for Bioengineering Research and Education, University of Calgary, Calgary, AB, Canada.
[5]Charbonneau Cancer Institute, University of Calgary, Calgary, AB, Canada.

Abstract

Processing bodies (PBs) are ribonucleoprotein granules important for cytokine mRNA decay that are targeted for disassembly by many viruses. Kaposi's sarcoma-associated herpesvirus is the etiological agent of the inflammatory endothelial cancer, Kaposi's sarcoma, and a PB-regulating virus. The virus encodes Kaposin B (KapB), which induces actin stress fibres (SFs) and cell spindling as well as PB disassembly. We now show that KapB-mediated PB disassembly requires actin rearrangements, RhoA effectors and the mechanoresponsive transcription activator, YAP. Moreover, ectopic expression of active YAP or exposure of ECs to mechanical forces caused PB disassembly in the absence of KapB. We propose that the viral protein KapB activates a novel mechanoresponsive signaling axis and links changes in cell shape and cytoskeletal structures to enhanced inflammatory molecule expression using PB disassembly. Our work implies that cytoskeletal changes in other pathologies will similarly impact the inflammatory environment.

Importance

For the first time, we demonstrate that processing bodies (PBs), cytoplasmic sites of RNA decay, are regulated by mechanical signaling events that alter actin dynamics. Using the overexpression of a viral protein called KapB, known previously to mediate PB disassembly, we show that actin stress fibers (SFs) and the mechanoresponsive transcription factor, YAP, are required for PB loss. We also show that other established mechanical signals (shear stress or stiff extracellular matrix) that lead to the formation of SFs and activate YAP also cause PB disassembly. This is important because it means that KapB activates, from the inside out, a pathway that links cell shape to post-transcriptional gene regulation via cytoplasmic PBs.

Introduction

Cells are exposed to a variety of environments and they respond to changes in external force by adjusting internal tension. These mechanical cues can be transmitted to the cell through changes to extracellular contact nodes (focal adhesions) and contractile actomyosin structures to maintain tension homeostasis (Friedland, Lee, and Boettiger 2009; Kong et al. 2009; del Rio et al. 2009; Grashoff et al. 2010; reviewed in Finch-Edmondson and Sudol 2016). Actin stress fibres (SFs) are cytoskeletal structures composed of thick actin bundles, often associated with focal adhesions (Vallenius 2013), that are force-responsive, maintaining cytoskeletal integrity in changing mechanical environments (Burridge and Guilluy 2016). SF formation is coordinated by the GTPase, RhoA; it activates the formin, mammalian diaphanous protein-1 (mDia1) to promote actin filament growth and Rho-associated coiled-coil kinase (ROCK) to promote actomyosin contractility through non-muscle myosin II (Watanabe et al. 1997; Amano et al. 1997; Kimura et al. 1996). These RhoA-effectors act together to promote the formation of contractile and stable actin filaments in response to mechanical and chemical stimuli (Watanabe et al. 1999).

External forces elicit a cascade of signals using actin as force transducers to alter gene expression. Activated serum response factor (SRF) transcription responds to actin polymerization (reviewed in Chai and Tarnawski 2002). SRF activation is negatively regulated by the cytoplasmic concentration of monomeric G-actin (Sotiropoulos et al. 1999). However, inducers of filamentous actin (e.g. active RhoA) deplete G-actin levels leading to SRF nuclear translocation and transcription (Sotiropoulos et al. 1999). A more recent example is the mechanoresponsive transcriptional coactivator Yes-associated protein (YAP), whose activity can be controlled by cell shape and cytoskeletal structure (Dupont et al. 2011; Wada et al. 2011; Halder, Dupont, and Piccolo 2012; Yu et al. 2012). YAP is nuclear and active in response to low cell-cell contact (Zhao et al. 2007), high stiffness of the extracellular matrix (ECM) (Dupont et al. 2011), in shear stress due to fluid flow (K.-C. Wang et al. 2016; Nakajima et al. 2017; Lai and Stainier 2017; H. J. Lee et al. 2017; Huang et al. 2016), or after G-protein coupled receptor (GPCR) activation (Yu et al. 2012). Most of these signals induce the activity of RhoA and promote the formation of SFs, (Noria et al. 2004; Lee and Kumar 2016), implicating actin cytoskeletal structures as requisite intermediates for YAP activation.

Nuclear YAP associates with its coactivators to mediate transcription of genes involved in cell proliferation, differentiation, survival and migration (Halder, Dupont, and Piccolo 2012).

57 Consistent with this, nuclear YAP is often pro-tumourigenic and drives progression of many
58 oncogenic traits in a variety of cancers. These include the induction of cell stemness (Panciera et
59 al. 2016), altered metabolism (C. Yang et al. 2018), cancer cell invasion/vascular remodeling
60 (Calvo et al. 2013; Liu et al. 2018; Kimura et al. 2020), and altered growth and proliferation
61 (Kapoor et al. 2014; Zanconato et al. 2015; Jang et al. 2017). Kaposi's sarcoma (KS) is an
62 endothelial cell (EC) cancer that is strongly linked to Kaposi's sarcoma-associated herpesvirus
63 (KSHV) (Chang et al. 1994; Russo et al. 1996; Zhong et al. 1996; Ganem 1997). KSHV
64 establishes persistent, life-long infection of its human host, and displays two types of infection,
65 latent and lytic. In KS, the majority of the tumour ECs are latently infected while lytic replication
66 is rare; in part, because these cells die as a result of viral replication (Boshoff et al. 1995; Staskus
67 et al. 1997; Umbach et al. 2010; Speck and Ganem 2010; Arias et al. 2014). That said, during
68 their short lifetime lytic cells expel progeny virus and secrete large quantities of pro-
69 inflammatory and angiogenic molecules, making even infrequent lytic replication an important
70 driver of KS. A key contributor to this secretory phenotype is the constitutively active viral G
71 protein-coupled receptor (vGPCR), a lytic viral protein (Montaner et al. 2006; Corcoran et al.
72 2012). Despite the paracrine contributors like vGPCR, the few gene products that are expressed
73 during the KSHV latent cycle are central for viral tumourigenesis. Many features of *in vivo* KS
74 are recapitulated by *in vitro* latent infection of primary ECs, or ectopic expression of individual
75 KSHV latent genes, including enhanced proliferation and an elongated or 'spindled' morphology
76 characteristic of KS. Spindling is induced by two KSHV latent genes, vFLIP (Grossmann et al.
77 2006) and Kaposin B (KapB; (Corcoran, Johnston, and McCormick 2015)). Spindled cells also
78 secrete a variety of proinflammatory cytokines and angiogenic factors, to further promote tumour
79 progression through inflammatory cytokine production (Ensoli 1998; Ciufo et al. 2001; Naranatt
80 et al. 2003; Grossmann et al. 2006; Ojala and Schulz 2014). However, no information exists to
81 demonstrate pro-tumourigenic YAP activation in KSHV latency, despite the fact that the vGPCR
82 has been shown to activate YAP during KSHV lytic infection (Liu et al. 2015).
83 One way that KSHV latency promotes the pro-inflammatory and pro-tumourigenic KS
84 microenvironment is via KapB-mediated disassembly of cytoplasmic ribonucleoprotein granules
85 called processing bodies (PBs) (Corcoran, Johnston, and McCormick 2015). PBs are involved in
86 many RNA regulatory processes such as RNA silencing, nonsense-mediated decay and mRNA
87 decay (Eulalio, Behm-Ansmant, and Izaurralde 2007). We and others have shown that PBs are

88 the major site for the translational suppression or constitutive decay of human mRNAs that code
89 for potent regulatory molecules such as proinflammatory cytokines (Franks and Lykke-Andersen
90 2007; Corcoran, Johnston, and McCormick 2015; Vindry et al. 2017; Blanco et al. 2014). There
91 are ~4500 of these transcripts, all of which bear destabilizing AU-rich elements (AREs) in their
92 3'-untranslated regions (3'-UTRs) (Shaw and Kamen 1986; Shyu, Greenberg, and Belasco 1989;
93 Chen and Shyu 1995; Winzen et al. 1999; Stoecklin, Mayo, and Anderson 2006; Franks and
94 Lykke-Andersen 2007; Bakheet, Williams, and Khabar 2006; Bakheet, Hitti, and Khabar 2017).
95 PB abundance and composition is extremely dynamic and responds to cellular stress (Sheth
96 2003; Kedersha and Anderson 2007; Aizer et al. 2008; Takahashi et al. 2011). Specifically,
97 activation of the stress-responsive p38/MK2 MAP kinase pathway by KapB elicits PB
98 disassembly and prevents constitutive ARE-mRNA turnover (Winzen et al. 1999; Docena et al.
99 2010; Corcoran et al. 2012; Corcoran and McCormick 2015; Corcoran, Johnston, and
100 McCormick 2015). This is an important yet underappreciated regulatory mechanism that fine
101 tunes the production of potent proinflammatory cytokines and angiogenic factors in KS.
102 Though PBs are dynamic and stress-responsive, the precise signaling events that lead to
103 PB assembly or disassembly are not well understood. We showed previously that KapB binds
104 and activates MK2, which then phosphorylates hsp27, complexes with p115RhoGEF, and
105 activates RhoA to elicit PB disassembly (Corcoran, Johnston, and McCormick 2015; Garcia et
106 al. 2009; McCormick and Ganem 2005). While it is well-established that RhoA coordinates SF
107 formation (Ridley and Hall 1992; Watanabe et al. 1999; Schmitz et al. 2000; Hotulainen and
108 Lappalainen 2006), the precise mechanism of how RhoA promotes PB disassembly is not
109 appreciated (Corcoran, Johnston, and McCormick 2015; Takahashi et al. 2011). In an effort to
110 better understand the regulation of PB disassembly by KapB and RhoA, we began by targeting
111 downstream RhoA effectors reported to promote SF formation to determine if the proteins
112 known to mediate cytoskeletal remodeling were also necessary for PB disassembly. We reasoned
113 that at some point we would be able to uncouple the signaling events that led to SFs from those
114 that led to PB disassembly. We were not. We now present data that conclusively shows KapB-
115 mediated PB disassembly is dependent not only on RhoA, but on cytoskeletal structures,
116 actomyosin contractility and the presence of the mechanoresponsive transcription transactivator,
117 YAP. We also present the first evidence of elevated YAP levels in response to expression of a
118 KSHV latent gene, KapB. We also extend these studies beyond their impact on viral

119 tumourigenesis, by determining the mechanical regulation of PB dynamics in the absence of
120 KapB expression, and show that induced cell contractility, cytoskeletal structures and active
121 YAP all precede PB disassembly. Using a viral protein from an oncogenic virus, we have
122 discovered a novel mechanoresponsive signaling pathway that transduces signals from cell shape
123 and cytoskeletal structures to YAP to control PBs, post-transcriptional regulators of cellular gene
124 expression.
125
126 **Results**
127 **RhoA effectors controlling SF formation are required for PB disassembly**
128 We previously showed that KapB-mediated PB disassembly required RhoA (Corcoran,
129 Johnston, and McCormick 2015). In this work, we investigated whether downstream RhoA
130 effectors known to control SF formation also control PB disassembly. Mammalian diaphanous
131 protein 1 (mDia1) and Rho-associated coiled-coil kinase (ROCK) are considered the main
132 coordinators of RhoA-mediated SF formation (Watanabe et al. 1999; Tojkander, Gateva, and
133 Lappalainen 2012). mDia1 is a formin that promotes actin filament polymerization (Watanabe et
134 al. 1999). To examine whether mDia1 was required for KapB-mediated PB disassembly, we
135 designed short hairpin RNAs (shRNAs) to silence mDia1 mRNA. KapB- and vector- expressing
136 human umbilical vein endothelial cells (HUVECs) were transduced with mDia1-targeting
137 shRNAs and selected. Silencing efficacy was confirmed with immunoblotting (Fig 1A). PB
138 analysis was performed using CellProfiler to quantify immunofluorescence images stained for
139 the hallmark PB-resident protein, Hedls, as described in detail in the methods (J. H. Yu et al.
140 2005; Kedersha et al. 2008). Knockdown of mDia1 increased PBs in KapB-expressing cells (Fig
141 1B, D). mDia1-sh1 showed a greater increase in PBs in comparison to mDia1-sh2 (Fig 1B),
142 likely because mDia1-sh1 reduced protein expression by 90% whereas mDia1-sh2 reduced it by
143 40-50% (Fig 1A). To ensure that the loss of mDia1 did not increase PBs globally but rather that
144 mDia1 contributed specifically to KapB-mediated PB disassembly, we calculated the ratio of
145 PBs per cell in KapB-expressing cells and normalized to PBs per cell in vector controls. This is
146 important because this calculation shows whether KapB is still able to disassemble PBs, relative
147 to vector, in the context of mDia silencing. If the ratio is ≥1 after sh-mDia treatment, it indicates
148 that KapB is no longer able to disassemble PBs in comparison to the vector control, and that
149 mDia contributes directly to KapB-mediated PB disassembly. Conversely, if the ratio is ~ 0.4 to

150 0.6, it indicates that KapB can still disassemble PBs even in the context of sh-mDia treatment. In
151 this case, we determined that silencing using both mDia1-sh1 and mDia1-sh2 restored the PB
152 ratio in KapB:Vector cells to ~1, indicating that the ability of KapB to disassemble PBs is lost
153 after mDia silencing and that this is a specific effect (Fig 1C). We note that this ratio will be
154 reported in subsequent figures for every RNA silencing or drug treatment applied to test KapB-
155 mediated PB disassembly. We also observed that mDia1 silencing did not eliminate SF
156 formation (Fig 1D) but, instead, increased elongated cells with visible actin SFs across the cell in
157 both vector and KapB conditions. The visible actin structures may represent different SF
158 subtypes or actin bundles that compensate for the loss of mDia1 (Hotulainen and Lappalainen
159 2006).
160 ROCK promotes SF formation by increasing actin contractility and inhibiting actin severing
161 activity (Julian and Olson 2014). Chemical inhibition of both isoforms of ROCK, ROCK1 and
162 ROCK2, with Y-27632 (Ishizaki et al. 2000) restored PBs in KapB-expressing cells and
163 increased the ratio of KapB:Vector PBs (Fig 2A-C). To determine whether PB disassembly is
164 dependent on a single ROCK isoform, both ROCK1 and ROCK2 were knocked down with
165 isoform-specific shRNAs. Knockdown efficacy was confirmed with immunoblotting (Fig S1).
166 Independent knockdown of ROCK1 and 2 increased PBs counts in KapB-expressing cells (Fig
167 2D, F) and restored the ratio of KapB:Vector PBs counts (Fig 2E). This indicated that both
168 ROCK1 and ROCK2 can contribute to KapB-mediated PB disassembly. ROCK2 knockdown
169 showed more robust PB restoration, both in terms of PB counts and PB size, than that seen with
170 ROCK1 knockdown (Fig 2D, F). Quantification of PB counts in control cells for both pan-
171 ROCK inhibition and ROCK knockdown experiments is reported in Figure S1. While pan-
172 ROCK inhibition and ROCK1 knockdown treatments both eliminate SFs, ROCK2 knockdown
173 retains pronounced actin fibres in the cells (Fig 2F). Similar to mDia1 knockdown, this may
174 indicate a compensatory mechanism to retain cell shape and suggests that only a subset of SFs
175 may be required for PB disassembly. Taken together, these data show that inhibition of RhoA
176 effectors that mediate SF formation can reverse KapB-mediated PB disassembly. Put another
177 way, we have been unable to uncouple KapB-mediated SF formation from KapB-mediated PB
178 disassembly.
179 ROCK phosphorylates and activates LimK, which then phosphorylates and inactivates
180 cofilin, an actin-severing protein (Ohashi et al. 2000). In this way, ROCK promote SF formation.

181 To investigate the role of cofilin in KapB-mediated PB disassembly, shRNAs to knockdown
182 cofilin expression were used (Fig S2A). Since ROCK activation results in less cofilin activity
183 and reduced actin severing, we hypothesized that knockdown of cofilin in KapB-expressing cells
184 would augment KapB-mediated PB disassembly. Knockdown of cofilin resulted in elongated
185 cells with more SFs (Fig S2D). Cofilin knockdown also augmented PBs disassembly in KapB-
186 expressing cells (Fig S2B, C). This indicates that inhibition of cofilin elicits PB disassembly and
187 supports the hypothesis that by reducing cofilin activity to promote KapB-mediated SF
188 formation, PB disassembly is enhanced.
189
190 **G-actin concentration does not influence PB disassembly**
191 Since we could not uncouple the signalling controlling SF formation from PB
192 disassembly, we investigated whether changes in the concentration of monomeric G-actin,
193 known to control cellular stress and SRF transcriptional responses (Sotiropoulos et al. 1999;
194 Chambers et al. 2015), could be controlling PBs. Several studies have shown that increasing the
195 proportion of filamentous actin decreases the cytoplasmic concentration of monomeric G-actin
196 (Rasmussen et al. 2010; Bunnell et al. 2011; Chambers et al. 2015). We investigated if our
197 phenotype, PB disassembly, was controlled by changes in the proportion of monomeric G-actin.
198 To determine this, cells were treated with drugs known to either decrease or increase the
199 proportion of monomeric G-actin. Jasplakinolide (Jasp) treatment decreases the G-actin fraction
200 by facilitating actin nucleation and aberrant polymerization of actin (Bubb et al. 1999).
201 Conversely, the actin polymerization inhibitor Cytochalasin D (CytD) caps the barbed end of
202 actin filaments, preventing further elongation of the actin filament and increasing the free G-
203 actin concentration (Wakatsuki et al. 2001). If the level of G-actin is the signal, we hypothesized
204 that jasplakinolide, which decreases G-actin levels, would mediate PB disassembly, while
205 cytochalasin D would do the opposite, and promote PB assembly. However, both treatments
206 increased the PB count per cell (Fig S3A-C); these data indicate that the concentration of G-actin
207 does not influence PB disassembly, and this is not the mechanism by which actin SF formation
208 or enhanced activity of RhoA alters PB dynamics. These data are congruent with our mDia1 and
209 ROCK knockdown experiments that show retention of visible F-actin bundles despite PB
210 restoration.
211

212 **α −actinin-1 activity promotes PB disassembly**

213 The actinins are primarily known for their role in bundling actin fibres, though in non-
214 muscle cells, α -actinin-1 and 4 do not mediate actin bundling to the same extent (Pellegrin and
215 Mellor 2007). α -actinin-4 can, at times, localize to dorsal SFs, but it primarily mediates focal
216 adhesion turnover and can act as a transcriptional regulator of genes associated with cell
217 proliferation and differentiation (Honda et al. 1998; Kovac 2010; Honda 2015). α -actinin-1
218 primarily mediates SF bundling and formation, as well as focal adhesion maturation (Honda et
219 al. 1998; Kovac 2010). Using immunofluorescence, we observed that the localization of the two
220 isoforms seen in HUVECs (Fig S4A, B) was consistent with the reported localization and
221 function, as α -actinin-1 was localized to actin fibres and α -actinin-4 was more diffusely
222 cytoplasmic and nuclear, with some actin fibre localization (Honda et al. 1998; Kovac 2010).
223 Since α -actinin-1 associated with SFs in HUVECs and overexpression of alpha-actinin-GFP has
224 been shown to localize and reinforce SFs (Edlund, Lotano, and Otey 2001; Jackson et al. 2008),
225 we asked whether its overexpression would promote PB disassembly. This was indeed the case,
226 suggesting that enhancing SF bundling and focal adhesion maturation positively regulates PB
227 disassembly (Fig S4C, D).
228

229 **Changes in cytoskeletal contractility control PB disassembly**

230 One of the downstream activities of the kinase, ROCK, is to phosphorylate myosin light
231 chain to induce non-muscle myosin II (NMII)-mediated actomyosin contraction (Mutsuki
232 Amano et al. 1996). Since ROCK is required for KapB-mediated PB disassembly, we
233 determined whether functional actomyosin contractility is also required. KapB-expressing cells
234 were treated with blebbistatin, which inhibits NMII-mediated actomyosin contractility by
235 maintaining NMII in a conformation that is unable to bind actin filaments (Kovacs et al. 2004).
236 Treatment of KapB-expressing cells with blebbistatin restored both PBs levels in KapB-
237 expressing cells, as well as the KapB:Vector ratio of PBs (Fig 3A-C), indicating that
238 contractility is required for KapB-induced PB disassembly. To determine if contraction would
239 elicit the same phenotype in the absence of KapB, cells were treated with Calyculin A (CalA),
240 an inhibitor of myosin light chain phosphatase that promotes NMII phosphorylation and
241 actomyosin contraction (Asano and Mabuchi 2001). Inducing contraction with CalA decreased

242 counts of PBs (Fig 3D, E), again consistent with the hypothesis that actomyosin contractility
243 controls PB disassembly.
244 Actomyosin contractility impacts cytoskeletal tension in adherent cells with SFs (Katoh
245 et al. 1998; Tan et al. 2003). Additionally, both Jasp and CytD interfere with cytoskeletal
246 tension (Rotsch and Radmacher 2000), and both increased PB counts (Fig S3). Since the
247 mechanoresponsive transcription activator, YAP, is activated by increases to cytoskeletal
248 tension via actomyosin contractility (Dupont et al. 2011), we predicted the following: 1) KapB
249 expression increases cytoskeletal tension, 2) KapB expression will activate YAP and 3) both
250 cytoskeletal tension and YAP will be required for PB disassembly. Though unable to directly
251 test the first prediction, we now consider the role of YAP in KapB-mediated PB disassembly.
252
253 **YAP activation induces PB disassembly**
254 We investigated the cellular localization of YAP in KapB-expressing cells. KapB-
255 transduced human umbilical vein endothelial cells (HUVECs) showed increased levels of
256 nuclear YAP, as well as increased total YAP intensity by immunofluorescence, though the ratio
257 of nuclear:cytoplasmic YAP was not markedly increased (Fig 4A). When YAP is phosphorylated
258 by LATS, it is sequestered in the cytoplasm and transcriptionally inactive (Zhao et al. 2007).
259 While YAP has multiple phosphorylation sites, phosphorylation at serine 127 is the most potent
260 LATS-mediated phosphorylation site that promotes cytoplasmic distribution of YAP (Zhao et al.
261 2007). To investigate the phosphorylation status of YAP in KapB-expressing cells, levels of
262 P(S127)-YAP and total YAP were measured by immunoblot. In KapB-expressing cells, there
263 was a decrease in the ratio of P(S127)-YAP to total YAP suggesting that YAP is active when
264 KapB is expressed (Fig 4B). We also observed an increase in total steady-state levels of YAP by
265 immunoblotting, corroborating the increase in total YAP intensity seen by microscopy (Fig 4A,
266 B). Taken together, these observations are the first evidence of enhanced YAP activity in
267 response to expression of a KSHV latent gene. We next asked if active YAP in KapB-expressing
268 cells can interact with TEAD and other transcription factors to elicit changes in gene expression
269 (Vassilev et al. 2001). We used a TEAD-element luciferase assay to assess if canonical YAP
270 transcription was activated. As a positive control, we used YAP 5SA, a mutant version of YAP
271 that is unable to be phosphorylated and inactivated by the inhibitory kinase LATS (Zhao et al.
272 2007) and is thus considered constitutively active. YAP 5SA robustly activated the TEAD

273 element-containing firefly luciferase reporter (Fig S5A). Despite our observations of increased
274 nuclear and total YAP, KapB did not induce the transcription of the TEAD element-containing
275 firefly luciferase reporter (TEAD-Fluc; Fig S5A). Further, KapB did not increase steady-state
276 mRNA levels of common YAP target genes CTGF, CYR61 and ANKRD1 by RT-qPCR,
277 although these genes were elevated by YAP 5SA (Fig S5B). These data indicate despite the
278 observation that YAP appears more abundant and nuclear in KapB-expressing cells, it is not
279 activating transcription of its canonical gene targets.
280 We expressed shRNAs targeting YAP in KapB-expressing HUVECs to assess whether
281 the altered levels of YAP impacted PB disassembly. Immunoblotting confirmed knockdown
282 efficiency (Fig 4C). Knockdown of YAP increased PBs in KapB-expressing cells (Fig 4D-F). In
283 the context of YAP knockdown, the KapB:Vector ratio of PBs counts was restored, indicating
284 that YAP is required for KapB-mediated PB disassembly (Fig 4E) and suggesting that KapB is
285 activating a mechanoresponsive signalling axis to elicit PB disassembly via YAP. We wondered
286 if YAP was central to PB disassembly in the absence of KapB expression. To this end, we
287 examined PBs after YAP 5SA expression. These cells displayed decreased number of PBs per
288 cell, indicating that YAP 5SA elicited disassembly of PBs (Fig 5A, B). KapB-mediated PB
289 disassembly correlates with increases in stability and levels of ARE-mRNA (Corcoran, Johnston,
290 and McCormick 2015; McCormick and Ganem 2005). To examine whether YAP 5SA-mediated
291 PB disassembly elicits the same changes in ARE-mRNAs, we used a luciferase assay previously
292 established to measure the stability of ARE-mRNAs by measuring luminescence of an ARE-
293 containing firefly luciferase reporter (Corcoran, Khaperskyy, and McCormick 2011). In this
294 assay, as previously shown in Corcoran, Johnston, and McCormick (2015), KapB increased level
295 of firefly luminescence indicating enhanced stability of its RNA transcript (Fig 5C). However,
296 despite also inducing pronounced PB disassembly, YAP 5SA does not increase Fluc
297 luminescence significantly more than the control construct (Fig 5C). This points to a divergence
298 of KapB and active YAP outcome. Although PB disassembly is induced by the expression of
299 both constitutively active YAP and KapB, active YAP increases the transcriptional activation of
300 genes CTGF, CYR61 and ANKRD1 while KapB does not; conversely, KapB enhances the
301 stability of ARE-mRNAs while active YAP does not.
302
303 **YAP activators disassemble PBs**

304 Since overexpression of constitutively active YAP leads to disassembly of PBs, we
305 wanted to determine whether activation of endogenous YAP could do the same in the absence of
306 KapB. We tested various upstream mechanical signals described to activate YAP for their ability
307 to elicit PB disassembly: shear stress, low cell confluence and high ECM stiffness (Nakajima et
308 al. 2017; Lee et al. 2017; Noria et al. 2004; Zhao et al. 2007; Dupont et al. 2011). For the first,
309 we subjected HUVECs to shear stress by fluid flow (shear forces of 2 and 10 dyn/cm^2) and PBs
310 were examined via immunofluorescence. Both treatments showed prominent cell elongation and
311 resulted in robust PB disassembly (Fig 6A, B). To test if cell confluence regulates PB levels,
312 HUVECs were seeded at low, medium and high densities. Cells at low confluence are reported to
313 have active YAP and we predicted PBs would disassembly; however, the low-density monolayer
314 displayed more PBs per cell then those at medium and high densities (Fig 6C, D). To test the
315 impact of collagen stiffness on PB disassembly, HUVECs were plated on coverslips coated with
316 increasing densities of collagen (0 to 64 μg/ cm^2). While collagen density does not perfectly
317 reproduce matrix stiffness as it does not eliminate effects from increasing collagen-binding sites,
318 increasing collagen densities correlate with increases in matrix stiffness (Yang, Leone, and
319 Kaufman 2009; Lee et al. 2014; Joshi, Mahajan, and Kothapalli 2018). As collagen density
320 increased, PBs decreased (Fig 6E, F). Taken together, these data indicate that PB disassembly
321 occurred in response to mechanical stimuli known to require RhoA and altered cytoskeletal
322 structures to activate YAP (shear stress and increased ECM concentration) (Zhao et al. 2012;
323 Huang et al. 2016; Lee and Kumar 2016; Moreno-Vicente et al. 2018). Again, our model points
324 to the importance of actin SF formation as a requisite precursor to PB disassembly irrespective of
325 YAP activation status.
326
327 **Shear stress mediated PB disassembly requires YAP**
328 YAP responds to external forces that induce active RhoA, actin SFs, and pronounced cell
329 elongation; in short, the typical behaviour of ECs in response to fluid flow. However, how YAP
330 responds to shear stress is controversial (Wang et al. 2016; Huang et al. 2016; Lee et al. 2017;
331 Nakajima and Mochizuki 2017). To verify YAP activation by continuous, unidirectional fluid
332 flow in our system, HUVECs subjected to 2 and 10 dyn/cm^2 of shear stress were lysed and used
333 for immunoblotting for P(S127)-YAP and total YAP. Shear stress the ratio of phosphor-
334 YAP/YAP in both conditions, suggesting a higher proportion of active YAP (Fig 7A). To assess

335 if YAP was required for PB disassembly in response to shear stress, HUVECs transduced with
336 YAP-targeting shRNA were subjected to 10 dyn/cm^2 shear stress. PBs disassembled in cells
337 treated with a non-targeting shRNA when subjected to shear stress (Fig 7B, C), consistent with
338 earlier experiments (Fig 6A, B). When YAP was reduced by shRNA expression, ECs exposed to
339 shear stress had more PBs than control cells without shear (Fig 7B, C). Therefore, YAP is
340 required to disassemble PBs in response to shear stress. Taken together with our analysis of
341 KapB-mediated PB disassembly, these data suggest that when KapB is expressed, it turns on the
342 same mechanoresponsive signals that endothelial cells use to withstand mechanical forces like
343 shear, in the absence of an external stimulus. The outcome of both scenarios is YAP-dependent
344 disassembly of cytoplasmic PBs.
345
346 **Discussion**
347 In this manuscript, we have used a viral protein from an oncogenic virus to uncover the
348 relationship between cytoplasmic PBs and the mechanical regulation of actin SF formation. We
349 present data to support the existence of a novel mechanoresponsive pathway that links actin SFs,
350 actomyosin contractility, and the transcription transactivator YAP to the disassembly of PBs and
351 show that this pathway is hijacked by KapB during KSHV latency. Our major findings are as
352 follows. i) KapB-mediated PB disassembly requires actin SF effectors ROCK1/2 /mDia1 and is
353 enhanced by loss of the actin-severing protein, cofilin. ii) KapB-mediated PB disassembly is
354 reversed when blebbistatin is used to inhibit actomyosin contractility or after knockdown of the
355 mechanoresponsive transcription transactivator, YAP. iii) In the absence of KapB, we can induce
356 PB disassembly when we promote the formation of actin SFs, actomyosin contractility, and YAP
357 activity using overexpression of α−actinin-1 (promotes actin bundling into SFs and increases
358 cytoskeletal tension (Jackson et al. 2008)), Calyculin A (inhibits myosin light chain phosphatase
359 to promote actomyosin contraction (Asano and Mabuchi 2001)), or overexpression of active
360 YAP (YAP 5SA). Exposure of endothelial cells to the external forces created by shear stress or a
361 stiff extracellular matrix also induces PB disassembly in the absence of KapB. Together, these
362 data show for the first time, that PBs disassemble in response to mechanical signals that
363 transduce external forces from outside the cell to the actin cytoskeleton and that this is a pathway
364 used by endothelial cells to regulate gene expression in response to diverse stimuli. Moreover,
365 this work also highlights the remarkable pizzazz used by viruses to hijack cellular pathways. In

366 this case, we reveal that the viral protein KapB taps into this mechanoresponsive pathway to
367 trigger mechanical changes to cytoskeletal structures and downstream effectors that would
368 normally respond to force, thereby inducing PB disassembly from within the cell, rather than
369 from without.

370 During the process of actin polymerization, the monomeric form of actin, globular actin
371 (G-actin), aggregates in groups of three subunits or more to nucleate an actin filament, which
372 extends into filaments via addition of further G-actin monomers through ATP-dependent
373 polymerization (reviewed in Pollard 2016). 10 to 30 actin filaments (F-actin) bundle together
374 into SFs, primarily using the α-actinin family for crosslinking (Small et al. 1998; Cramer,
375 Siebert, and Mitchison 1997; Lazarides and Burridge 1975; Pellegrin and Mellor 2007). SFs with
376 periodic distribution of actin-crosslinking proteins and non-muscle myosin II (NMII) are
377 contractile structures (Katoh et al. 1998; Tan et al. 2003), but not all actin SFs function equally in
378 this regard. For any structure to be able to generate tension, it must be tethered at the ends. Of the
379 types of SFs (ventral SFs, dorsal SFs and transverse arcs; (Small et al. 1998)), ventral SFs are
380 attached at both termini to the extracellular matrix (ECM) through focal adhesions and contain
381 NMII, which imparts a contractile phenotype (Hotulainen and Lappalainen 2006; Small et al.
382 1998; Vallenius 2013). Dorsal SFs are attached through focal adhesions but do not contain NMII,
383 and thus are not contractile (Small et al. 1998; Vallenius 2013). However, dorsal SFs are thought
384 to work in concert with transverse arcs, which contain NMII but are not attached to focal
385 adhesions, to mediate cellular contractility.

386 In this work, while we did not directly determine the subtype of actin SF structures that
387 form in response to KapB-mediated RhoA activation, several features of our data suggest that the
388 structures that are important for PB disassembly must be contractile and cytoskeletal tension.
389 When both mDia1 and ROCK2 were silenced in KapB-expressing cells (Fig 1, 2), visible actin
390 bundles are still apparent despite PB restoration in both contexts. This suggests that not all SF
391 subtypes are required for our phenotype. In addition, blebbistatin treatment of KapB-expressing
392 cells dramatically restored PBs; these data suggest that PB disassembly requires actin-mediated
393 contractility rather than merely structural support (Fig 3). Furthermore, overexpression of α-
394 actinin and shear stress increase cell stiffness (Lee et al. 2006; Jackson et al. 2008). Both
395 treatments induced PB disassembly (Fig S4, 6), reinforcing the correlation between increasing
396 cell tension and PB disassembly. Finally, our data show that YAP is required for PB disassembly

397 (Figs 4, 5, 7). YAP is mechanoresponsive; it becomes active when tension-forming actin
398 structures are induced by external forces e.g. focal adhesion engagement by stiff ECM (Dupont
399 et al. 2011; Sugimoto et al. 2018). As YAP activation and PB disassembly both rely on RhoA-
400 induced cytoskeletal contractility, any activator of YAP that induces cytoskeletal tension through
401 RhoA should mediate PB disassembly. Our data supports this notion, as shear stress forces and
402 increasing collagen density both cause PB disassembly in the absence of KapB, while low
403 confluence does not (Fig 6). We also know that GPCRs ($G_{11/12}$ and $G_{q/}$11) activate YAP in a
404 RhoA-dependent manner (Yu et al. 2012) and LPA treatment or overexpression of KSHV-
405 derived constitutively active vGPCR (both activate $G_{11/12}$) both induce PB disassembly (Corcoran
406 et al. 2012; Corcoran and McCormick 2015), these findings support the conclusion that PB
407 disassembly requires the formation of contractile actin structures like those associated with YAP
408 transactivation responses.
409 KSHV is an oncogenic virus associated with the endothelial neoplasm, Kaposi's sarcoma
410 (KS). Cells within the KS lesion display latent KSHV infection, proliferate abnormally, spindle,
411 and release many pro-inflammatory and pro-tumourigenic mediators into the microenvironment.
412 KapB expression alone recapitulates two of these key features, cell spindling and pro-
413 inflammatory mediator production that results from enhanced stability of ARE-containing
414 cytokine mRNAs that would normally shuttle to PBs for constitutive turnover (Corcoran,
415 Johnston, and McCormick 2015). Our previous work showed that both phenotypes require KapB
416 activation of the stress-responsive kinase, MK2, and the downstream activation of the GTPase
417 RhoA (Corcoran, Johnston, and McCormick 2015; Corcoran and McCormick 2015). We also
418 showed that the lytic vGPCR protein mediates PB disassembly and the concomitant stabilization
419 of ARE-mRNAs; more recently ORF57 has been also reported to disrupt PBs (Corcoran et al.
420 2012; Sharma et al. 2019). The observation that KSHV encodes at least three separate gene
421 products sufficient to drive PB disassembly suggests that PB disassembly is beneficial for some
422 aspect of the infectious cycle. Further research is required to definitively address how PBs
423 influence the KSHV infectious cycle and the fate of infected cells.
424 We and others observed that the presence or absence of PB punctae visible by
425 microscopy directly correlates with the stability of ARE-mRNAs (Corcoran, Johnston, and
426 McCormick 2015; Vindry et al. 2017; Blanco et al. 2014). We predicted that YAP- mediated PB
427 disassembly would also promote ARE-mRNA stability. Indeed, several YAP-target genes

428 contain ARE elements in their 3'UTR, including CTGF and ANKRD1 (Shen and Stanger 2015;
429 Bakheet, Hitti, and Khabar 2017). Shear forces also cause YAP-dependent PB disassembly and
430 have previously been shown to upregulate many genes containing ARE-mRNAs (Vozzi et al.
431 2018; Bakheet, Hitti, and Khabar 2017). Comparison of the transcriptomic data from HUVECs
432 subjected to shear stress from Vozzi et al (2018) (Accession: GEO, GSE45225) to entries in the
433 ARE-mRNA database (Bakheet, Hitti, and Khabar 2017) showed a 20% enrichment in the
434 proportion of genes that contained AREs in those transcripts that were upregulated by shear
435 stress. This suggests that PB disassembly enables efficient translation of YAP targets by
436 preventing recruitment of the ARE-containing transcripts to PBs. That said, overexpression of
437 constitutively active YAP (YAP 5SA) disassembles PBs but does not increase stability of an
438 ARE-containing firefly luciferase reporter (Fig 5) (Corcoran, Khaperskyy, and McCormick
439 2011)). This discrepancy may be due to different functional responses for different classes of
440 AU-rich elements. Our ARE-containing luciferase reporter contains the AU-rich sequence
441 derived from the 3'-UTR of GM-CSF, categorized in Cluster 5, whereas canonical YAP genes
442 CTGF and ANKDR1 are in Clusters 1 and 2, respectively (Bakheet, Hitti, and Khabar 2017).
443 Data presented herein clearly implicate a requirement for YAP in the PB disassembly
444 phenotype that is induced by KapB and by the external force, shear stress (Fig 4,7). However, the
445 precise connection between YAP and PB disassembly is unclear. What we do know is that
446 despite the clear reliance on YAP for PB disassembly, KapB does not increase expression of
447 canonical YAP-regulated transcripts (Fig S5). Our data also show increases in total YAP,
448 decreases in phosphorylated YAP; however, the ratio of nuclear:cytoplasmic YAP is not
449 markedly altered (Fig 4). Taken together, these data suggest that PB disassembly is independent
450 of YAP's role as a gene transactivator and may also be independent of YAP nuclear
451 translocation. In the discussion that follows, we explore two possible models for how YAP may
452 promote PB disassembly that are independent of its transactivation of canonical genes. *i)*
453 *Cytoplasmic YAP promotes autophagic flux to promote PB catabolism*. Several studies link YAP
454 with the regulation of the catabolic process of autophagy, though many of these are contradictory
455 and suggest YAP-mediated autophagy control is cell type and context-dependent (Song et al.
456 2015; Liu et al. 2017; Pei et al. 2019; Totaro et al. 2019). Totaro et al. provided strong evidence
457 to support that YAP promotes autophagic flux by promoting the expression of Armus, a Rab7-
458 GAP that is required to mediate the fusion of autophagosomes with lysosomes in the final

459 degradative step of autophagy (Totaro et al. 2019). Their data also show that autophagic flux is a
460 mechanoresponsive process; this supported by other studies wherein endothelium exposed to
461 unidirectional shear stress upregulates autophagy (Liu et al. 2015; Yao et al. 2015; Wang et al.
462 2018; Das et al. 2018). These data are also consistent with preliminary data from our group that
463 suggests that PB disassembly mediated by KapB requires autophagy (knockdown of Atg5
464 restores PBs [Robinson, Singh, Corcoran, unpublished data]) and the work of others (Hardy et al.
465 2017). In this model, we propose that the intermediate step(s) linking the requirement of YAP to
466 the disappearance of PBs is the upregulation of autophagic flux, which results in the autophagic
467 degradation of PB granules or PB components. *ii) YAP and PBs are antiviral* PBs are sites
468 where innate immune factors congregate that are disrupted by most viruses during infection
469 (Burdick et al. 2010; Li et al. 2012; Ostareck, Naarmann-de Vries, and Ostareck-Lederer 2014;
470 Burgess and Mohr 2015; Cuevas et al. 2016; H. Wang et al. 2016; Lumb et al. 2017; Balinsky et
471 al. 2017; Núñez et al. 2018; Ng et al. 2020). Indeed, KSHV encodes three separate proteins that
472 all induce PB disassembly (Corcoran et al. 2012; Corcoran, Johnston, and McCormick 2015;
473 Sharma et al. 2019). PBs are likely playing an as yet undefined and underappreciated role in
474 regulating innate antiviral responses. YAP is also a novel and unappreciated negative regulator
475 of innate immune signaling pathways. YAP blocks the ability of the innate immune kinase,
476 TBK1, a downstream effector for several innate signaling pathways, to associate and activate its
477 substrates (Zhang et al 2017). In so doing, YAP blocks downstream induction of interferons and
478 increases viral replication (Zhang et al. 2017). This feature of YAP is independent of its ability to
479 act as a transcriptional transactivator (Zhang et al. 2017). We speculate that KapB-induced PB
480 disassembly, like active YAP, favours viral replication and survival and is promoted by KSHV in
481 order to reshape subsequent antiviral innate immune responses.
482 In this manuscript, we describe the surprising convergence of two previously unrelated
483 yet essential regulators of cellular gene expression – the mechanoresponsive transactivator YAP
484 and cytoplasmic PBs, known regulators of AU-rich mRNA decay. We show that PB disassembly
485 is mechanoresponsive; external forces that change cell shape and tension-forming cytoskeletal
486 structures cause PB disassembly in a YAP-dependent manner. This discovery was made courtesy
487 of the unique KSHV protein, KapB, and provides yet another example of how viruses have
488 evolved surprising ways to manipulate their host and ensure their survival. In this case, KapB
489 induces, from the inside out, a mechanoresponsive pathway to cause PB disassembly and

490 elevated YAP. Future study will untangle how these related mechanoresponsive events are
491 induced by KSHV to better promote viral replication.
492
493 **Materials and Methods**
494 **Antibodies, Plasmids and Reagents**
495 The antibodies used in this study can be found in Table S1. The plasmids used in this
496 study can be found in Table S2. Forward and reverse shRNA sequences were selected from the
497 TRC Library Database in the Broad Institute RNAi consortium. YAP target shRNAs in pLKO.1
498 were obtained from Dr. C. McCormick (Dalhousie University, Halifax, Canada). Sequences for
499 all shRNA oligonucleotides used for cloning are listed in Table S3. Cloning of shRNAs was
500 conducted according to the pLKO.1 protocol (Addgene 2006). The chemical inhibitors used in
501 this study can be found in Table S4.
502 **Cell Culture**
503 Human embryonic kidney 293T and 293A cells (HEK-293T/A, ATCC, Manassas,
504 Virginia, US) and human cervical adenocarcinoma cells expressing a tetracycline-inducible
505 repressor (HeLa Tet-Off, Clontech, Mountain View, California, US) were cultured in Dulbecco's
506 Modified Eagle Medium (DMEM, Gibco, Carlsbad, California, US) supplemented with 10%
507 heat-inactivated fetal bovine serum (Gibco), 100 U/mL penicillin, 100 μg/mL streptomycin, and
508 2 mM L-glutamine (Gibco). Pooled human umbilical vein endothelial cells (HUVECs, Lonza,
509 Basel, Switzerland) were cultured in endothelial cell growth medium 2 (EGM-2, Lonza)). For
510 HUVEC passaging, tissue culture plates were precoated for 30 min at 37˚C with 0.1% (w/v)
511 porcine gelatin (Sigma, St. Louis, Missouri, US) in 1X PBS (Gibco).
512 **Transfection for Lentivirus Production**
513 HEK-293T cells at 70-80% confluence were transfected using 3.3 μg of the target
514 lentiviral construct, 2 μg pSPAX2 and 1 μg pMD2.G with 1 mg/mL polyethyenimine (PEI,
515 Sigma) in serum-free DMEM. After 5 to 6 h, media was replaced with antibiotic-free DMEM
516 containing 10% FBS and 2 mM L-glutamine (Gibco). Transfected cells were incubated for 48 h
517 at 37˚C to allow lentivirus production. The supernatant media containing viral particles was
518 harvested and filtered through a 0.45 μm polyethersulfone (PES) filter (VWR, Randor,
519 Pennsylvania, US) and aliquoted. Virus was stored at -80˚C until use.
520 **Lentiviral Transduction**

521 Lentivirus was supplied into wells of plated HUVECs in EGM-2 supplemented with 5
522 μg/mL hexadimethrine bromide (polybrene). After 24 h incubation, cells were selected with
523 either 5 μg/mL blasticidin (Sigma) for 96 h, replacing the media and antibiotic at 48 h, or 1
524 μg/mL puromycin (Sigma) for 48 h. Following selection, HUVEC medium was replaced with
525 EGM-2 without selection for at least 24 h recovery before further use.

526 **Immunofluorescence**

527 Immunofluorescence was performed as described previously (Corcoran, Johnston, and
528 McCormick 2015). Briefly, cells were grown on coverslips (no. 1.5, Electron Microscopy
529 Sciences, Hatfield, Pennsylvania, US). Following treatment, coverslips were fixed in 4%
530 paraformaldehyde (PFA, Electron Microscopy Sciences) in PBS at 37°C for 10 min,
531 permeabilized with 0.1% Triton-X100 (Sigma) in 1X PBS for 10 min at RT, and blocked in 1%
532 Human AB serum (blocking buffer, Sigma) in 1X PBS for 1 h at RT. Coverslips were then
533 incubated with diluted primary antibody in blocking buffer overnight at 4°C in a humidified
534 chamber. After primary antibody incubation, coverslips were washed with 1X PBS and then
535 incubated in fluorescently-tagged secondary antibody diluted in blocking buffer for 1 h at RT. If
536 applicable, coverslips were stained with Phalloidin-conjugated Alexa-Fluor 647 (Invitrogen,
537 1:100) in 1X PBS for 1.5 h. Coverslips were mounted onto microscope slides (FisherBrand,
538 Pittsburgh, Pennsylvania, US) using Prolong Gold Antifade Mounting Media (Invitrogen,
539 Carlsbad, California, US). For coverslips that were used for Hedls puncta quantification, the
540 following modifications to immunofluorescence were made: (1) Prior to permeabilization,
541 coverslips were stained with wheat germ agglutinin (WGA) Alexa-647 conjugate (Invitrogen,
542 1:400) in 1X PBS for 10 min at RT. (2) Following secondary antibody incubation, coverslips
543 were stained with 4',6-Diamidino-2-Phenylindole (DAPI, Invitrogen, 1:10,000) in 1X PBS for 5
544 min.

545 Confocal imaging was performed on the Zeiss LSM 880 Confocal Microscope
546 (Charbonneau Microscopy Facility, University of Calgary, Calgary, Canada) at the 63X oil
547 objective. CellProfiler imaging was performed on the Zeiss AxioImager Z2 (CORES facility,
548 Dalhousie University, Halifax, Canada) or Zeiss AxioObserver (Charbonneau Microscopy
549 Facility, University of Calgary) at the 40X oil objective.

550 **Quantification of Processing Bodies Using CellProfiler Analysis**

551 CellProfiler (cellprofiler.org) is an open source software for high-content image analysis
552 (Kamentsky et al. 2011) and was used to develop an unbiased method for quantifying changes to
553 PB dynamics. The pipeline used for quantifying PBs was structured as follows: To detect nuclei,
554 the DAPI image was thresholded into a binary image. In the binary image, primary objects
555 between 30 to 200 pixels in diameter were detected and defined as nuclei. Cells were identified
556 as secondary objects in the WGA image using a propagation function from the identified nuclei,
557 which determined the cell's outer edge. Using the parameters of a defined nucleus and cell
558 border, the cytoplasm was then defined as a tertiary object. The Hedls channel image was
559 enhanced using an "Enhance Speckles" function to identify distinct puncta and eliminate
560 background staining. The cytoplasm image was then applied as a mask to the enhanced puncta
561 image to ensure quantitation of only cytoplasmic puncta. Hedls puncta were measured in the
562 cytoplasm of cells using a 'global thresholding with robust background adjustments' function as
563 defined by the program. The threshold cut-off for identified Hedls puncta remained constant
564 between all experiments with identical staining parameters. Puncta number per cell, intensity and
565 locations with respect to the nucleus were measured and exported as .csv files and analyzed in
566 RStudio. A template of the RStudio analysis pipeline is attached in Appendix A. Data was
567 represented as fold change in Hedls puncta count per cell normalized to the vector puncta count.
568 'Relative Hedls Puncta/Cell (KapB/Vector)' demonstrates the KapB puncta count divided by
569 vector puncta count, a ratio that was calculated within each treatment group for each biological
570 replicate.
571
572 **Protein Electrophoresis and Immunoblotting**
573 Cells were lysed in 2X Laemmli buffer (20% glycerol, 4% SDS, 120 mM Tris-HCl),
574 between 150 to 300 μL, depending on cell density. Lysates were homogenized with a 0.21-gauge
575 needle, and supplemented to contain 0.02% (w/v) bromophenol blue (Sigma) and 0.05 M
576 dithiothreitol (DTT, Sigma), then heated at 95˚C for 5 min. 7.5 or 12% TGX Stain-Free SDS-
577 polyacrylamide gels (BioRad) were cast according to the instructions of the manufacturer and 5
578 to 15 μg of total protein were subjected to SDS gel electrophoresis using 1X SDS running buffer
579 (25 mM Tris, 192 mM Glycine, 0.1% SDS). Precision Plus Protein All Blue Prestained Protein
580 Standards (BioRad, Hercules, California, US) was used as a molecular weight marker. After
581 electrophoresis, gels were UV-activated using the ChemiDocTouch (BioRad) Stain-Free Gel

582 setting with automated exposure for 45 s. The protein was transferred to low-fluorescence
583 polyvinylidene difluoride (PVDF) membranes (BioRad) on the Trans-Blot Turbo Transfer
584 System (BioRad) according to the instructions of the manufacturer. Following transfer, total
585 protein amounts on membranes were imaged on the ChemiDocTouch using the Stain-Free
586 Membrane setting with automated exposure. Membranes were then blocked using 5% BSA
587 (Sigma) in 1X TBS-T (150 nM NaCl, 10 mM Tris, pH 7.8, 0.01% Tween-20) for 1 h at RT.
588 Primary antibody was diluted in 2.5% BSA in 1X TBS-T. Membranes were incubated in
589 primary antibody solution overnight at 4°C with rocking. The following day, membranes were
590 washed 3 times for 5 min in 1X TBS-T. Membranes were incubated with the appropriate
591 secondary antibody, conjugated to horseradish peroxidase (HRP) for 1 h at RT. Membranes were
592 washed 4 times for 5 min in 1X TBS-T. Clarity™ Western ECL Blotting Substrate (BioRad) was
593 mixed at a 1:1 ratio and applied to the membrane for 5 min. Chemiluminescent signal was
594 imaged on ChemiDocTouch Chemiluminescence setting. Band intensity was quantified using
595 ImageLab software (BioRad), normalizing to total protein.

596 **Quantitative Reverse-Transcriptase Polymerase Chain Reaction (qRT-PCR)**

597 Cells were lysed in 250 μL RLT buffer (Qiagen, Hilden, Germany) and RNA was
598 extracted using the RNeasy Plus Mini kit (Qiagen) according to the manufacturer's instructions.
599 Complementary DNA (cDNA) was synthesized from 1 μg of total RNA using the qScript cDNA
600 SuperMix (QuantaBio, Hilden, Germany) according to the manufacturer's instructions. Real-
601 time quantitative PCR with SsoFast EvaGreen qPCR MasterMix (BioRad) was used to quantify
602 the fold-change in mRNA abundance. Relative fluorescence was quantified using CFX Connect
603 (BioRad). All qRT-PCR primers efficiencies were between 90-110% in HUVECs and sequences
604 are found in Table S5.

605 **Luciferase Assay for TEAD Transcriptional Activity**

606 HEK-293A cells were seeded in antibiotic-free DMEM at 75,000 cells/well. Mixtures of
607 500 ng of the target construct (pcDNA (Vector), pcDNA-KapB (KapB), p1XFLAG or
608 p2XFLAG-YAP 5SA), 450 ng 8X-GTIIC luciferase reporter, 50 ng TREX-Renilla luciferase
609 reporter and 3 μL FuGENE HD Transfection Reagent (Promega, Madison, Wisconsin, US) were
610 transfected into HEK-293A cells. After 36 h, DMEM containing only 2 mM L-glutamine
611 (starvation media) was supplied to the cells. Twelve hours after addition of starvation media,
612 cells were lysed in 200 μL passive lysis buffer (Promega) and luciferase activity was assayed

613 using the Dual-Luciferase Reporter Assay System (Promega) according to the manufacturer's
614 instructions. Luminescence was measured using the GloMax Luminometer (Promega).

615 **Luciferase Assay for Stability of mRNA with AU-Rich Elements**

616 This technique is described in Corcoran, Khaperskyy, and McCormick (2011). Briefly,
617 Hela-Tet Off cells were seeded in antibiotic-free DMEM at 100,000 cells/well. Mixtures of 900
618 ng of the target construct (pcDNA (Vector), pcDNA-KapB (KapB), p1XFLAG or p2XFLAG-
619 YAP 5SA), 90 ng TREX-Firefly ARE luciferase, 10 ng TREX-Renilla luciferase and 3 μL
620 FuGENE HD Transfection Reagent (Promega) were transfected into Hela Tet-Off cells. After 36
621 h, 1 μg/mL doxycycline was supplied to the cells to inhibit further transcription of each reporter.
622 Twelve hours after addition of doxycycline, cells were lysed in 200 μL passive lysis buffer
623 (Promega) and luciferase activity was assayed using the Dual-Luciferase Reporter Assay System
624 (Promega) according to the manufacturer's instructions. Luminescence was measured using the
625 GloMax Luminometer (Promega).

626 **Collagen-Coating for Altering Matrix Stiffness**

627 Coverslips (no. 1.5, Electron Microscopy Sciences) were coated with a dilution series (0
628 to 64 μg/cm^2) of rat-tail collagen-1 (Gibco) in 0.02 M acetic acid for 4 h at RT. Slides were
629 sterilized with UV irradiation and washed with 2 times with sterile 1X PBS prior to seeding
630 cells.

631 **Unidirectional Fluid Flow for Endothelial Cell Shear Stress**

632 A parallel-plate flow chamber was used to expose ECs to shear stress. The system was
633 described in detail in Gomez-Garcia et al. (2018). Briefly, cleaned, unfrosted microscope slides
634 (Cole-Parmer, Vernon Hills, Illinois, US) were coated for 4 h at RT with rat-tail collagen-1
635 (Gibco) in 0.02 M acetic acid for a resultant 8.3 μg/cm^2 collagen density. Slides were sterilized
636 with UV irradiation and washed 2 times with sterile 1X PBS. HUVECs were seeded at a density
637 of 350,000 cells/slide and cultured for 24 h. Forty-five mL of EGM-2 supplemented with dextran
638 (Spectrum Chemical, New Brunswick, New Jersey, US) for a resultant 3 cP viscosity was added
639 to the stock media bottle. The stock media bottle was connected with the associated tubing and
640 pulse dampener. Slides with seeded cells were inserted onto the flow chamber, a gasket
641 (Specialty Manufacturing, Calgary, Canada) was added, and the system was sealed shut and
642 attached to the flow loop following the outlet of a pulse dampener. The rate of fluid flow was
643 started at 0.3 L/min and doubled every 15 min until final flow rates of 0.6 L/min and 2.7 L/min

644 were reached, corresponding to shear stress rates of 2 and 10 dyn/cm^2. Following 21 h, cells were
645 removed and immediately fixed for immunofluorescence or lysed for immunoblotting.

646 **Statistical Analysis**

647 Statistical analysis was performed in GraphPad Prism 8.0 software. Significance was
648 determined using a ratio paired t-test or repeated measures analysis of variance (ANOVA). One-
649 tailed ratio paired t-tests were applied in comparisons specifically examining PB restoration in
650 KapB-expressing cells as a directional hypothesis. In all other comparisons, two-tailed ratio
651 paired t-tests were applied. Significance was determined at $p = 0.05$. Each biological replicate
652 for CellProfiler quantification consisted of 6 images of each treatment in a given experiment,
653 counting approximately 100 to 200 cells per treatment.
654

655 **References**

656 Aizer, Adva, Yehuda Brody, Lian Wee Ler, Nahum Sonenberg, Robert H. Singer, and Yaron
657 Shav-Tal. 2008. "The Dynamics of Mammalian P Body Transport, Assembly, and
658 Disassembly In Vivo." *Molecular Biology of the Cell* 19 (11): 4154–66.
659 https://doi.org/10.1091/mbc.E08.

660 Amano, M, K Chihara, K Kimura, Y Fukata, N Nakamura, Y Matsuura, and K Kaibuchi. 1997.
661 "Formation of Actin Stress Fibers and Focal Adhesions Enhanced by Rho-Kinase." *Science*
662 275 (5304): 1308–11. https://doi.org/10.1126/science.275.5304.1308.

663 Amano, Mutsuki, Masaaki Ito, Kazushi Kimura, Yuko Fukata, Kazuyasu Chihara, Takeshi
664 Nakano, Yoshiharu Matsuura, and Kozo Kaibuchi. 1996. "Phosphorylation and Activation
665 of Myosin by Rho-Associated Kinase (Rho-Kinase)." *The Journal of Biological Chemistry*
666 271 (34): 20246–49. https://doi.org/10.1074/jbc.271.34.20246.

667 Arias, Carolina, Ben Weisburd, Noam Stern-Ginossar, Alexandre Mercier, Alexis S. Madrid,
668 Priya Bellare, Meghan Holdorf, Jonathan S. Weissman, and Don Ganem. 2014. "KSHV 2.0:
669 A Comprehensive Annotation of the Kaposi's Sarcoma-Associated Herpesvirus Genome
670 Using Next-Generation Sequencing Reveals Novel Genomic and Functional Features."
671 *PLoS Pathogens* 10 (1). https://doi.org/10.1371/journal.ppat.1003847.

672 Asano, Yukako, and Issei Mabuchi. 2001. "Calyculin-A, an Inhibitor for Protein Phosphatases,
673 Induces Cortical Contraction in Unfertilized Sea Urchin Eggs." *Cell Motility and the*
674 *Cytoskeleton* 48 (4): 245–61. https://doi.org/10.1002/cm.1013.

675 Bakheet, Tala, Edward Hitti, and Khalid S A Khabar. 2017. "ARED-Plus: An Updated and
676 Expanded Database of AU-Rich Element-Containing MRNAs and Pre-MRNAs." *Nucleic*
677 *Acids Research* 46 (October 2017): 2017–19. https://doi.org/10.1093/nar/gkx975.

678 Bakheet, Tala, Bryan R G Williams, and Khalid S a Khabar. 2006. "ARED 3.0: The Large and
679 Diverse AU-Rich Transcriptome." *Nucleic Acids Research* 34 (Database issue): D111–14.
680 https://doi.org/10.1093/nar/gkj052.

681 Balinsky, Corey A., Hana Schmeisser, Alexandra I. Wells, Sundar Ganesan, Tengchuan Jin,
682 Kavita Singh, and Kathryn C. Zoon. 2017. "IRAV (FLJ11286), an Interferon-Stimulated
683 Gene with Antiviral Activity against Dengue Virus, Interacts with MOV10." Edited by
684 Michael S. Diamond. *Journal of Virology* 91 (5). https://doi.org/10.1128/JVI.01606-16.

685 Blanco, Fernando F, Sandhya Sanduja, Natasha G Deane, Perry J Blackshear, and Dan a Dixon.

686 2014. “Transforming Growth Factor β Regulates P-Body Formation through Induction of
687 the MRNA Decay Factor Tristetraprolin.” *Molecular and Cellular Biology* 34 (2): 180–95.
688 https://doi.org/10.1128/MCB.01020-13.
689 Boshoff, Chris, Thomas F Schulz, Margaret M Kennedy, Andrew K Graham, Cyril Fisher, Alero
690 Thomas, J O’D. McGee, Robin a Weiss, and John J O’Leary. 1995. “Kaposi’s Sarcoma-
691 Associated Herpesvirus Infects Endothelial and Spindle Cells.” *Nature Medicine* 1 (12):
692 1274–78. https://doi.org/10.1038/nm1295-1274.
693 Bubb, Michael R, Ilan Spector, Bret B Beyer, and Katina M. Fosen. 2000. “Effects of
694 Jasplakinolide on the Kinetics of Actin Polymerization.” *Journal of Biological Chemistry*
695 275 (7): 5163–70. https://doi.org/10.1074/jbc.275.7.5163.
696 Bunnell, Tina M., Brandon J. Burbach, Yoji Shimizu, and James M. Ervasti. 2011. “β-Actin
697 Specifically Controls Cell Growth, Migration, and the G-Actin Pool.” Edited by Paul
698 Forscher. *Molecular Biology of the Cell* 22 (21): 4047–58. https://doi.org/10.1091/mbc.e11-
699 06-0582.
700 Burdick, Ryan, Jessica L. Smith, Chawaree Chaipan, Yeshitila Friew, Jianbo Chen, Narasimhan
701 J. Venkatachari, Krista A. Delviks-Frankenberry, Wei-Shau Hu, and Vinay K. Pathak.
702 2010. “P Body-Associated Protein Mov10 Inhibits HIV-1 Replication at Multiple Stages.”
703 *Journal of Virology* 84 (19): 10241–53. https://doi.org/10.1128/jvi.00585-10.
704 Burgess, Hannah M., and Ian Mohr. 2015. “Cellular 5′-3′ MRNA Exonuclease Xrn1 Controls
705 Double-Stranded RNA Accumulation and Anti-Viral Responses.” *Cell Host and Microbe*
706 17 (3): 332–44. https://doi.org/10.1016/j.chom.2015.02.003.
707 Burridge, Keith, and Christophe Guilluy. 2016. “Focal Adhesions, Stress Fibers and Mechanical
708 Tension.” *Experimental Cell Research* 343 (1): 14–20.
709 https://doi.org/10.1016/j.yexcr.2015.10.029.
710 Calvo, Fernando, Nil Ege, Araceli Grande-Garcia, Steven Hooper, Robert P. Jenkins, Shahid I.
711 Chaudhry, Kevin Harrington, et al. 2013. “Mechanotransduction and YAP-Dependent
712 Matrix Remodelling Is Required for the Generation and Maintenance of Cancer-Associated
713 Fibroblasts.” *Nature Cell Biology* 15 (6): 637–46. https://doi.org/10.1038/ncb2756.
714 Chai, J., and Andrzej S. Tarnawski. 2002. “Serum Response Factor: Discovery, Biochemistry,
715 Biological Roles and Implications for Tissue Injury Healing.” *Journal of Physiology and*
716 *Pharmacology* 53 (2): 147–57. https://doi.org/10.1007/s12630-011-9636-x.

717 Chambers, Joseph E, Lucy E Dalton, Hanna J Clarke, Elke Malzer, Caia S Dominicus, Vruti
718 Patel, Greg Moorhead, David Ron, and Stefan J Marciniak. 2015. "Actin Dynamics Tune
719 the Integrated Stress Response by Regulating Eukaryotic Initiation Factor 2α
720 Dephosphorylation." *ELife* 4 (March). https://doi.org/10.7554/eLife.04872.
721 Chang, Y, E Cesarman, M S Pessin, F Lee, J Culpepper, D M Knowles, and P S Moore. 1994.
722 "Identification of Herpes-like DNA Sequences in AIDS-Associated Kaposi's Sarcoma."
723 *Science* 266: 1865–69. https://doi.org/10.1126/science.7997879.
724 Chen, C Y, and a B Shyu. 1995. "AU-Rich Elements: Characterization and Importance in
725 MRNA Degradation." *Trends in Biochemical Sciences* 20 (11): 465–70.
726 https://doi.org/10.1016/S0968-0004(00)89102-1.
727 Ciufo, D M, J S Cannon, L J Poole, F Y Wu, P Murray, R F Ambinder, and G S Hayward. 2001.
728 "Spindle Cell Conversion by Kaposi's Sarcoma-Associated Herpesvirus: Formation of
729 Colonies and Plaques with Mixed Lytic and Latent Gene Expression in Infected Primary
730 Dermal Microvascular EndCiufo, D. M., Cannon, J. S., Poole, L. J., Wu, F. Y., Murray,
731 P.,." *Journal of Virology* 75 (12): 5614–26. https://doi.org/10.1128/JVI.75.12.5614-
732 5626.2001.
733 Corcoran, Jennifer A., Benjamin P. Johnston, and Craig McCormick. 2015. "Viral Activation of
734 MK2-Hsp27-P115RhoGEF-RhoA Signaling Axis Causes Cytoskeletal Rearrangements, P-
735 Body Disruption and ARE-MRNA Stabilization." Edited by Erle S. Robertson. *PLoS*
736 *Pathogens* 11 (1): e1004597. https://doi.org/10.1371/journal.ppat.1004597.
737 Corcoran, Jennifer A., Denys A. Khaperskyy, Benjamin P. Johnston, Christine A. King, David P.
738 Cyr, Alisha V. Olsthoorn, and Craig McCormick. 2012. "Kaposi's Sarcoma-Associated
739 Herpesvirus G-Protein-Coupled Receptor Prevents AU-Rich-Element-Mediated MRNA
740 Decay." *Journal of Virology* 86 (16): 8859–71. https://doi.org/10.1128/JVI.00597-12.
741 Corcoran, Jennifer A., Denys A. Khaperskyy, and Craig McCormick. 2011. "Assays for
742 Monitoring Viral Manipulation of Host ARE-MRNA Turnover." *Methods* 55 (2): 172–81.
743 https://doi.org/10.1016/j.ymeth.2011.08.005.
744 Corcoran, Jennifer A, and Craig McCormick. 2015. "Viral Activation of Stress-Regulated Rho-
745 GTPase Signaling Pathway Disrupts Sites of MRNA Degradation to Influence Cellular
746 Gene Expression." *Small GTPases* 6 (4): 178–85.
747 https://doi.org/10.1080/21541248.2015.1093068.

748 Cramer, Louise P., Margaret Siebert, and Timothy J. Mitchison. 1997. "Identification of Novel
749 Graded Polarity Actin Filament Bundles in Locomoting Heart Fibroblasts: Implications for
750 the Generation of Motile Force." *Journal of Cell Biology* 136 (6): 1287–1305.
751 https://doi.org/10.1083/jcb.136.6.1287.
752 Cuevas, Rolando A., Arundhati Ghosh, Christina Wallerath, Veit Hornung, Carolyn B. Coyne,
753 and Saumendra N. Sarkar. 2016. "MOV10 Provides Antiviral Activity against RNA Viruses
754 by Enhancing RIG-I–MAVS-Independent IFN Induction." *The Journal of Immunology* 196
755 (9): 3877–86. https://doi.org/10.4049/jimmunol.1501359.
756 Das, Joyjyoti, Somnath Maji, Tarun Agarwal, Suman Chakraborty, and Tapas K. Maiti. 2018.
757 "Hemodynamic Shear Stress Induces Protective Autophagy in HeLa Cells through Lipid
758 Raft-Mediated Mechanotransduction." *Clinical and Experimental Metastasis* 35 (3): 135–
759 48. https://doi.org/10.1007/s10585-018-9887-9.
760 Docena, G., L. Rovedatti, L. Kruidenier, Á Fanning, N. A.B. Leakey, C. H. Knowles, K. Lee, et
761 al. 2010. "Down-Regulation of P38 Mitogen-Activated Protein Kinase Activation and
762 Proinflammatory Cytokine Production by Mitogen-Activated Protein Kinase Inhibitors in
763 Inflammatory Bowel Disease." *Clinical and Experimental Immunology* 162 (1): 108–15.
764 https://doi.org/10.1111/j.1365-2249.2010.04203.x.
765 Dupont, Sirio, Leonardo Morsut, Mariaceleste Aragona, Elena Enzo, Stefano Giulitti,
766 Michelangelo Cordenonsi, Francesca Zanconato, et al. 2011. "Role of YAP/TAZ in
767 Mechanotransduction." *Nature* 474 (7350): 179–83. https://doi.org/10.1038/nature10137.
768 Edlund, Magnus, Marc A. Lotano, and Carol A. Otey. 2001. "Dynamics of Alpha-Actinin in
769 Focal Adhesions and Stress Fibers Visualized with Alpha-Actinin-Green Fluorescent
770 Protein." *Cell Motility and the Cytoskeleton* 48 (3): 190–200. https://doi.org/10.1002/1097-
771 0169(200103)48:3<190::AID-CM1008>3.0.CO;2-C.
772 Ensoli, B. 1998. "Kaposi's Sarcoma: A Result of the Interplay among Inflammatory Cytokines,
773 Angiogenic Factors and Viral Agents." *Cytokine & Growth Factor Reviews* 9 (1): 63–83.
774 https://doi.org/10.1016/S1359-6101(97)00037-3.
775 Eulalio, Ana, Isabelle Behm-Ansmant, and Elisa Izaurralde. 2007. "P Bodies: At the Crossroads
776 of Post-Transcriptional Pathways." *Nature Reviews Molecular Cell Biology* 8 (1): 9–22.
777 https://doi.org/10.1038/nrm2080.
778 Finch-Edmondson, Megan, and Marius Sudol. 2016. "Framework to Function: Mechanosensitive

Regulators of Gene Transcription." *Cellular & Molecular Biology Letters* 21 (1): 28. https://doi.org/10.1186/s11658-016-0028-7.

Franks, Tobias M., and Jens Lykke-Andersen. 2007. "TTP and BRF Proteins Nucleate Processing Body Formation to Silence MRNAs with AU-Rich Elements." *Genes and Development* 21 (6): 719–35. https://doi.org/10.1101/gad.1494707.

Friedland, Julie C, Mark H Lee, and David Boettiger. 2009. "Mechanically Activated Integrin Switch Controls Alpha5 Beta1 Function." *Science* 323 (January): 642–44.

Ganem, Don. 1997. "KSHV and Kaposi's Sarcoma: The End of the Beginning?" *Cell* 91 (2): 157–60. https://doi.org/10.1016/S0092-8674(00)80398-0.

Garcia, Melissa C., Denise M. Ray, Brad Lackford, Mark Rubino, Kenneth Olden, and John D. Roberts. 2009. "Arachidonic Acid Stimulates Cell Adhesion through a Novel P38 MAPK-RhoA Signaling Pathway That Involves Heat Shock Protein 27." *Journal of Biological Chemistry* 284 (31): 20936–45. https://doi.org/10.1074/jbc.M109.020271.

Gomez-Garcia, M. Juliana, Amber L. Doiron, Robyn R. M. Steele, Hagar I. Labouta, Bahareh Vafadar, Robert D. Shepherd, Ian D. Gates, David T. Cramb, Sarah J. Childs, and Kristina D. Rinker. 2018. "Nanoparticle Localization in Blood Vessels: Dependence on Fluid Shear Stress, Flow Disturbances, and Flow-Induced Changes in Endothelial Physiology." *Nanoscale* 10 (32): 15249–61. https://doi.org/10.1039/C8NR03440K.

Grashoff, Carsten, Brenton D. Hoffman, Michael D. Brenner, Ruobo Zhou, Maddy Parsons, Michael T. Yang, Mark A. McLean, et al. 2010. "Measuring Mechanical Tension across Vinculin Reveals Regulation of Focal Adhesion Dynamics." *Nature* 466 (7303): 263–66. https://doi.org/10.1038/nature09198.

Grossmann, Claudia, Simona Podgrabinska, Mihaela Skobe, and Don Ganem. 2006. "Activation of NF-KB by the Latent VFLIP Gene of Kaposi's Sarcoma-Associated Herpesvirus Is Required for the Spindle Shape of Virus-Infected Endothelial Cells and Contributes to Their Proinflammatory Phenotype." *Journal of Virology* 80 (14): 7179–85. https://doi.org/10.1128/jvi.01603-05.

Halder, Georg, Sirio Dupont, and Stefano Piccolo. 2012. "Transduction of Mechanical and Cytoskeletal Cues by YAP and TAZ." *Nature Publishing Group* 13 (9): 591–600. https://doi.org/10.1038/nrm3416.

Hardy, Shana D., Aparna Shinde, Wen Horng Wang, Michael K. Wendt, and Robert L. Geahlen.

2017. “Regulation of Epithelial-Mesenchymal Transition and Metastasis by TGF-β, P-Bodies, and Autophagy.” *Oncotarget* 8 (61): 103302–14. https://doi.org/10.18632/oncotarget.21871.

Honda, K, T Yamada, R Endo, Y Ino, M Gotoh, H Tsuda, Y Yamada, H Chiba, and S Hirohashi. 1998. “Actinin-4, a Novel Actin-Bundling Protein Associated with Cell Motility and Cancer Invasion.[Erratum Appears in J Cell Biol 1998 Oct 5;143(1):Following 276].” *Journal of Cell Biology* 140 (6): 1383–93. https://doi.org/10.1083/jcb.140.6.1383.

Honda, Kazufumi. 2015. “The Biological Role of Actinin-4 (ACTN4) in Malignant Phenotypes of Cancer.” *Cell and Bioscience* 5 (1): 1–9. https://doi.org/10.1186/s13578-015-0031-0.

Hotulainen, Pirta, and Pekka Lappalainen. 2006. “Stress Fibers Are Generated by Two Distinct Actin Assembly Mechanisms in Motile Cells.” *Journal of Cell Biology* 173 (3): 383–94. https://doi.org/10.1083/jcb.200511093.

Huang, Yu, Li Wang, Jiang Yun Luo, Bochuan Li, Xiao Yu Tian, Li Jing Chen, Yuhong Huang, et al. 2016. “Integrin-YAP/TAZ-JNK Cascade Mediates Atheroprotective Effect of Unidirectional Shear Flow.” *Nature* 540 (7634): 579–82. https://doi.org/10.1038/nature20602.

Ishizaki, T, M Uehata, I Tamechika, J Keel, K Nonomura, M Maekawa, and S Narumiya. 2000. “Pharmacological Properties of Y-27632, a Specific Inhibitor of Rho-Associated Kinases.” *Molecular Pharmacology* 57 (5): 976–83. http://www.ncbi.nlm.nih.gov/pubmed/10779382.

Jackson, Wesley M., Michael J. Jaasma, Andrew D. Baik, and Tony M. Keaveny. 2008. “Over-Expression of Alpha-Actinin with a GFP Fusion Protein Is Sufficient to Increase Whole-Cell Stiffness in Human Osteoblasts.” *Annals of Biomedical Engineering* 36 (10): 1605–14. https://doi.org/10.1007/s10439-008-9533-9.

Jang, Wonyul, Tackhoon Kim, Ja Seung Koo, Sang-kyum Kim, and Dae-Sik Lim. 2017. “ Mechanical Cue-induced YAP Instructs Skp2-dependent Cell Cycle Exit and Oncogenic Signaling .” *The EMBO Journal* 36 (17): 2510–28. https://doi.org/10.15252/embj.201696089.

Joshi, Jyotsna, Gautam Mahajan, and Chandrasekhar R. Kothapalli. 2018. “Three-Dimensional Collagenous Niche and Azacytidine Selectively Promote Time-Dependent Cardiomyogenesis from Human Bone Marrow-Derived MSC Spheroids.” *Biotechnology and Bioengineering* 115 (8): 2013–26. https://doi.org/10.1002/bit.26714.

841 Julian, Linda, and Michael F Olson. 2014. "Rho-Associated Coiled-Coil Containing Kinases
842 (ROCK)." *Small GTPases* 5 (2): e29846. https://doi.org/10.4161/sgtp.29846.
843 Kamentsky, Lee, Thouis R Jones, Adam Fraser, Mark-Anthony Bray, David J Logan, Katherine
844 L Madden, Vebjorn Ljosa, Curtis Rueden, Kevin W Eliceiri, and Anne E Carpenter. 2011.
845 "Improved Structure, Function and Compatibility for CellProfiler: Modular High-
846 Throughput Image Analysis Software." *Bioinformatics (Oxford, England)* 27 (8): 1179–80.
847 https://doi.org/10.1093/bioinformatics/btr095.
848 Kapoor, Avnish, Wantong Yao, Haoqiang Ying, Sujun Hua, Alison Liewen, Qiuyun Wang, Yi
849 Zhong, et al. 2014. "Yap1 Activation Enables Bypass of Oncogenic KRAS Addiction in
850 Pancreatic Cancer." *Cell* 158 (1): 185–97. https://doi.org/10.1016/j.cell.2014.06.003.
851 Katoh, K., Y. Kano, M. Masuda, H. Onishi, and K. Fujiwara. 1998. "Isolation and Contraction of
852 the Stress Fiber." *Molecular Biology of the Cell* 9 (7): 1919–38.
853 https://doi.org/10.1091/mbc.9.7.1919.
854 Kedersha, Nancy, and Paul Anderson. 2007. "Mammalian Stress Granules and Processing
855 Bodies." *Methods in Enzymology* 431 (07): 61–81. https://doi.org/10.1016/S0076-
856 6879(07)31005-7.
857 Kedersha, Nancy, Sarah Tisdale, Tyler Hickman, and Paul Anderson. 2008. *Chapter 26 Real-*
858 *Time and Quantitative Imaging of Mammalian Stress Granules and Processing Bodies*.
859 *Methods in Enzymology*. 1st ed. Vol. 448. Elsevier Inc. https://doi.org/10.1016/S0076-
860 6879(08)02626-8.
861 Kimura, K, M Ito, M Amano, K Chihara, Y Fukata, M Nakafuku, B Yamamori, et al. 1996.
862 "Regulation of Myosin Phosphatase by Rho and Rho-Associated Kinase (Rho-Kinase)."
863 *Science (New York, N.Y.)* 273 (5272): 245–48.
864 https://doi.org/10.1126/science.273.5272.245.
865 Kimura, Masahiro, Takahiro Horie, Osamu Baba, Yuya Ide, Shuhei Tsuji, Randolph Ruiz
866 Rodriguez, Toshimitsu Watanabe, et al. 2020. "Homeobox A4 Suppresses Vascular
867 Remodeling by Repressing YAP/TEAD Transcriptional Activity." *EMBO Reports* 21 (4):
868 e48389. https://doi.org/10.15252/embr.201948389.
869 Kong, Fang, Andrés J. García, A. Paul Mould, Martin J. Humphries, and Cheng Zhu. 2009.
870 "Demonstration of Catch Bonds between an Integrin and Its Ligand." *Journal of Cell*
871 *Biology* 185 (7): 1275–84. https://doi.org/10.1083/jcb.200810002.

872 Kovac, Bianca. 2010. “Role and Function of Nonmuscle Alpha-Actinin-1 and -4 in Regulating
873 Distinct Subcategories of Actin Stress Fibers in Mammalian Cells.” University of Helsinki.
874 Kovacs, M., J. Toth, C. Hetenyi, A. Malnasi-Csizmadia, and J. R. Sellers. 2004. “Mechanism of
875 Blebbistatin Inhibition of Myosin II.” *Journal of Biological Chemistry* 279 (34): 35557–63.
876 https://doi.org/10.1074/jbc.M405319200.
877 Lai, Jason Kuan Han, and Didier Y.R. Stainier. 2017. “Pushing Yap into the Nucleus with Shear
878 Force.” *Developmental Cell* 40 (6): 517–18. https://doi.org/10.1016/j.devcel.2017.03.008.
879 Lazarides, Elias, and Keith Burridge. 1975. “α-Actinin: Immunofluorescent Localization of a
880 Muscle Structural Protein in Nonmuscle Cells.” *Cell* 6 (3): 289–98.
881 https://doi.org/10.1016/0092-8674(75)90180-4.
882 Lee, Byoungkoo, Xin Zhou, Kristin Riching, Kevin W. Eliceiri, Patricia J. Keely, Scott A.
883 Guelcher, Alissa M. Weaver, and Yi Jiang. 2014. “A Three-Dimensional Computational
884 Model of Collagen Network Mechanics.” Edited by Sanjay Kumar. *PLoS ONE* 9 (11):
885 e111896. https://doi.org/10.1371/journal.pone.0111896.
886 Lee, Hyun Jung, Miguel F. Diaz, Katherine M. Price, Joyce A. Ozuna, Songlin Zhang, Eva M.
887 Sevick-Muraca, John P. Hagan, and Pamela L. Wenzel. 2017. “Fluid Shear Stress Activates
888 YAP1 to Promote Cancer Cell Motility.” *Nature Communications* 8 (1): 14122.
889 https://doi.org/10.1038/ncomms14122.
890 Lee, J. S. H. 2006. “Ballistic Intracellular Nanorheology Reveals ROCK-Hard Cytoplasmic
891 Stiffening Response to Fluid Flow.” *Journal of Cell Science* 119 (9): 1760–68.
892 https://doi.org/10.1242/jcs.02899.
893 Lee, Stacey, and Sanjay Kumar. 2016. “Actomyosin Stress Fiber Mechanosensing in 2D and
894 3D.” *F1000Research* 5 (0): 2261. https://doi.org/10.12688/f1000research.8800.1.
895 Li, Ying, Rui Chen, Qian Zhou, Zhisheng Xu, Chao Li, Shuai Wang, Aiping Mao, Xiaodong
896 Zhang, Weiwu He, and Hong Bing Shu. 2012. “LSm14A Is a Processing Body-Associated
897 Sensor of Viral Nucleic Acids That Initiates Cellular Antiviral Response in the Early Phase
898 of Viral Infection.” *Proceedings of the National Academy of Sciences of the United States of*
899 *America* 109 (29): 11770–75. https://doi.org/10.1073/pnas.1203405109.
900 Liu, G., F. X. Yu, Y. C. Kim, Z. Meng, J. Naipauer, D. J. Looney, X. Liu, J. S. Gutkind, E. A.
901 Mesri, and K. L. Guan. 2015. “Kaposi Sarcoma-Associated Herpesvirus Promotes
902 Tumorigenesis by Modulating the Hippo Pathway.” *Oncogene* 34 (27): 3536–46.

903 https://doi.org/10.1038/onc.2014.281.
904 Liu, Huan, Xiaoming Dai, Xiaolei Cao, Huan Yan, Xinyan Ji, Haitao Zhang, Shuying Shen, et al.
905 2018. "PRDM4 Mediates YAP-induced Cell Invasion by Activating Leukocyte-specific
906 Integrin B2 Expression." *EMBO Reports* 19 (6): 1–14.
907 https://doi.org/10.15252/embr.201745180.
908 Liu, J., X. Bi, T. Chen, Q. Zhang, S. X. Wang, J. J. Chiu, G. S. Liu, Y. Zhang, P. Bu, and F.
909 Jiang. 2015. "Shear Stress Regulates Endothelial Cell Autophagy via Redox Regulation and
910 Sirt1 Expression." *Cell Death and Disease* 6 (7). https://doi.org/10.1038/cddis.2015.193.
911 Liu, Zeming, Wen Zeng, Shi Wang, Xiangwang Zhao, Yawen Guo, Pan Yu, Xingjie Yin,
912 Chunping Liu, and Tao Huang. 2017. "A Potential Role for the Hippo Pathway Protein,
913 YAP, in Controlling Proliferation, Cell Cycle Progression, and Autophagy in BCPAP and
914 KI Thyroid Papillary Carcinoma Cells." *American Journal of Translational Research* 9 (7):
915 3212–23.
916 Lumb, Jennifer H., Lauren M. Popov, Siyuan Ding, Marie T. Keith, Bryan D. Merrill, Harry B.
917 Greenberg, Jan E. Carette, Qin Li, and Jin Billy Li. 2017. "DDX6 Represses Aberrant
918 Activation of Interferon-Stimulated Genes." *Cell Reports* 20 (4): 819–31.
919 https://doi.org/10.1016/j.celrep.2017.06.085.
920 McCormick, Craig, and Don Ganem. 2005. "The Kaposin B Protein of KSHV Activates the
921 P38/MK2 Pathway and Stabilizes Cytokine MRNAs." *Science* 307 (5710): 739–41.
922 https://doi.org/10.1126/science.1105779.
923 Montaner, Silvia, Akrit Sodhi, Amanda K. Ramsdell, Daniel Martin, Jiadi Hu, Earl T. Sawai, and
924 J. Silvio Gutkind. 2006. "The Kaposi's Sarcoma-Associated Herpesvirus G Protein-Coupled
925 Receptor as a Therapeutic Target for the Treatment of Kaposi's Sarcoma." *Cancer*
926 *Research* 66 (1): 168–74. https://doi.org/10.1158/0008-5472.CAN-05-1026.
927 Moreno-Vicente, Roberto, Dácil María Pavón, Inés Martín-Padura, Mauro Català-Montoro,
928 Alberto Díez-Sánchez, Antonio Quílez-Álvarez, Juan Antonio López, et al. 2018.
929 "Caveolin-1 Modulates Mechanotransduction Responses to Substrate Stiffness through
930 Actin-Dependent Control of YAP." *Cell Reports* 25 (6): 1622-1635.e6.
931 https://doi.org/10.1016/j.celrep.2018.10.024.
932 Nakajima, Hiroyuki, and Naoki Mochizuki. 2017. "Flow Pattern-Dependent Endothelial Cell
933 Responses through Transcriptional Regulation." *Cell Cycle* 16 (20): 1893–1901.

934 https://doi.org/10.1080/15384101.2017.1364324.
935 Nakajima, Hiroyuki, Kimiko Yamamoto, Sobhika Agarwala, Kenta Terai, Hajime Fukui,
936 Shigetomo Fukuhara, Koji Ando, et al. 2017. "Flow-Dependent Endothelial YAP
937 Regulation Contributes to Vessel Maintenance." *Developmental Cell* 40 (6): 523-536.e6.
938 https://doi.org/10.1016/j.devcel.2017.02.019.
939 Naranatt, Pramod P., Shaw M. Akula, Christopher A. Zien, Harinivas H. Krishnan, and Bala
940 Chandran. 2003. "Kaposi's Sarcoma-Associated Herpesvirus Induces the
941 Phosphatidylinositol 3-Kinase-PKC-ζ-MEK-ERK Signaling Pathway in Target Cells Early
942 during Infection: Implications for Infectivity." *Journal of Virology* 77 (2): 1524–39.
943 https://doi.org/10.1128/jvi.77.2.1524-1539.2003.
944 Ng, Chen Seng, Dacquin M. Kasumba, Takashi Fujita, and Honglin Luo. 2020. "Spatio-
945 Temporal Characterization of the Antiviral Activity of the XRN1-DCP1/2 Aggregation
946 against Cytoplasmic RNA Viruses to Prevent Cell Death." *Cell Death and Differentiation*.
947 https://doi.org/10.1038/s41418-020-0509-0.
948 Noria, Sabrena, Feng Xu, Shannon McCue, Mara Jones, Avrum I Gotlieb, and B Lowell
949 Langille. 2004. "Assembly and Reorientation of Stress Fibers Drives Morphological
950 Changes to Endothelial Cells Exposed to Shear Stress." *The American Journal of Pathology*
951 164 (4): 1211–23. https://doi.org/10.1016/S0002-9440(10)63209-9.
952 Núñez, Rocío Daviña, Matthias Budt, Sandra Saenger, Katharina Paki, Ulrike Arnold, Anne
953 Sadewasser, and Thorsten Wolff. 2018. "The RNA Helicase DDX6 Associates with RIG-I
954 to Augment Induction of Antiviral Signaling." *International Journal of Molecular Sciences*
955 19 (7): 1–14. https://doi.org/10.3390/ijms19071877.
956 Ohashi, Kazumasa, Kyoko Nagata, Midori Maekawa, Toshimasa Ishizaki, Shuh Narumiya, and
957 Kensaku Mizuno. 2000. "Rho-Associated Kinase ROCK Activates LIM-Kinase 1 by
958 Phosphorylation at Threonine 508 within the Activation Loop." *Journal of Biological*
959 *Chemistry* 275 (5): 3577–82. https://doi.org/10.1074/jbc.275.5.3577.
960 Ojala, Päivi M., and Thomas F. Schulz. 2014. "Manipulation of Endothelial Cells by KSHV:
961 Implications for Angiogenesis and Aberrant Vascular Differentiation." *Seminars in Cancer*
962 *Biology* 26 (June): 69–77. https://doi.org/10.1016/j.semcancer.2014.01.008.
963 Ostareck, Dirk H., Isabel S. Naarmann-de Vries, and Antje Ostareck-Lederer. 2014. "DDX6 and
964 Its Orthologs as Modulators of Cellular and Viral RNA Expression." *Wiley Interdisciplinary*

965 *Reviews: RNA* 5 (5): 659–78. https://doi.org/10.1002/wrna.1237.
966 Panciera, Tito, Luca Azzolin, Atsushi Fujimura, Daniele Di Biagio, Chiara Frasson, Silvia
967 Bresolin, Sandra Soligo, et al. 2016. "Induction of Expandable Tissue-Specific
968 Stem/Progenitor Cells through Transient Expression of YAP/TAZ." *Cell Stem Cell* 19 (6):
969 725–37. https://doi.org/10.1016/j.stem.2016.08.009.
970 Pei, Tianjiao, Xin Huang, Ying Long, Changling Duan, Tingting Liu, Yujing Li, and Wei Huang.
971 2019. "Increased Expression of YAP Is Associated with Decreased Cell Autophagy in the
972 Eutopic Endometrial Stromal Cells of Endometriosis." *Molecular and Cellular*
973 *Endocrinology* 491 (April): 110432. https://doi.org/10.1016/j.mce.2019.04.012.
974 Pellegrin, S., and H. Mellor. 2007. "Actin Stress Fibres." *Journal of Cell Science* 120 (20):
975 3491–99. https://doi.org/10.1242/jcs.018473.
976 Pollard, Thomas D. 2016. "Actin and Actin-Binding Proteins." *Cold Spring Harbor Perspectives*
977 *in Biology* 8 (8): a018226. https://doi.org/10.1101/cshperspect.a018226.
978 Rasmussen, Izabela, Line H Pedersen, Luise Byg, Kazuhiro Suzuki, Hideki Sumimoto, and
979 Frederik Vilhardt. 2010. "Effects of F/G-Actin Ratio and Actin Turn-over Rate on NADPH
980 Oxidase Activity in Microglia." *BMC Immunology* 11 (1): 44. https://doi.org/10.1186/1471-
981 2172-11-44.
982 Ridley, Anne J., and Alan Hall. 1992. "The Small GTP-Binding Protein Rho Regulates the
983 Assembly of Focal Adhesions and Actin Stress Fibers in Response to Growth Factors." *Cell*
984 70 (3): 389–99. https://doi.org/10.1016/0092-8674(92)90163-7.
985 Rio, Armando del, Raul Perez-jimenez, Ruchuan Liu, Pere Roca-cusachs, Julio M Fernandez,
986 and Michael P Sheetz. 2009. "Stretching Single Talin Rod." *Science* 323 (5914): 638–41.
987 Rotsch, Christian, and Manfred Radmacher. 2000. "Drug-Induced Changes of Cytoskeletal
988 Structure and Mechanics in Fibroblasts: An Atomic Force Microscopy Study." *Biophysical*
989 *Journal* 78 (1): 520–35. https://doi.org/10.1016/S0006-3495(00)76614-8.
990 Russo, James J, Roy A Bohenzky, M.-C. Chien, Jing Chen, Ming Yan, Dawn Maddalena, J
991 Preston Parry, et al. 1996. "Nucleotide Sequence of the Kaposi Sarcoma-Associated
992 Herpesvirus (HHV8)." *Proceedings of the National Academy of Sciences* 93 (25): 14862–
993 67. https://doi.org/10.1073/pnas.93.25.14862.
994 Schmitz, Arndt A.P., Eve-Ellen Govek, Benjamin Böttner, and Linda Van Aelst. 2000. "Rho
995 GTPases: Signaling, Migration, and Invasion." *Experimental Cell Research* 261 (1): 1–12.

https://doi.org/10.1006/excr.2000.5049.

Sharma, Nishi R, Vladimir Majerciak, Michael J Kruhlak, Lulu Yu, Jeong Gu Kang, Acong Yang, Shuo Gu, Marvin J Fritzler, and Zhi-ming Zheng. 2019. "KSHV RNA-Binding Protein ORF57 Inhibits P-Body Formation to Promote Viral Multiplication by Interaction with Ago2 and GW182," 1–18. https://doi.org/10.1093/nar/gkz683.

Shaw, Gray, and Robert Kamen. 1986. "A Conserved AU Sequence from the 3′ Untranslated Region of GM-CSF MRNA Mediates Selective MRNA Degradation." *Cell* 46 (5): 659–67. https://doi.org/10.1016/0092-8674(86)90341-7.

Shen, Zhewei, and Ben Z. Stanger. 2015. "YAP Regulates S-Phase Entry in Endothelial Cells." Edited by Deanna M Koepp. *PLOS ONE* 10 (1): e0117522. https://doi.org/10.1371/journal.pone.0117522.

Sheth, Ujwal. 2003. "Decapping and Decay of Messenger RNA Occur in Cytoplasmic Processing Bodies." *Science* 300 (5620): 805–8. https://doi.org/10.1126/science.1082320.

Shyu, A. B., M. E. Greenberg, and J. G. Belasco. 1989. "The C-Fos Transcript Is Targeted for Rapid Decay by Two Distinct MRNA Degradation Pathways." *Genes & Development* 3 (1): 60–72. https://doi.org/10.1101/gad.3.1.60.

Small, J. Victor, K. Rottner, I. Kaverina, and K. I. Anderson. 1998. "Assembling an Actin Cytoskeleton for Cell Attachment and Movement." *Biochimica et Biophysica Acta - Molecular Cell Research* 1404 (3): 271–81. https://doi.org/10.1016/S0167-4889(98)00080-9.

Song, Qinghe, Beibei Mao, Jinbo Cheng, Yuhao Gao, Ke Jiang, Jun Chen, Zengqiang Yuan, and Songshu Meng. 2015. "YAP Enhances Autophagic Flux to Promote Breast Cancer Cell Survival in Response to Nutrient Deprivation." *PLoS ONE* 10 (3). https://doi.org/10.1371/journal.pone.0120790.

Sotiropoulos, Athanassia, Dziugas Gineitis, John Copeland, and Richard Treisman. 1999. "Signal-Regulated Activation of Serum Response Factor Is Mediated by Changes in Actin Dynamics." *Cell* 98 (2): 159–69. https://doi.org/10.1016/S0092-8674(00)81011-9.

Speck, Samuel H., and Don Ganem. 2010. "Viral Latency and Its Regulation: Lessons from the γ-Herpesviruses." *Cell Host and Microbe* 8 (1): 100–115. https://doi.org/10.1016/j.chom.2010.06.014.

Staskus, K A, W Zhong, K Gebhard, B Herndier, H Wang, R Renne, J Beneke, et al. 1997.

1027 "Kaposi's Sarcoma-Associated Herpesvirus Gene Expression in Endothelial (Spindle)
1028 Tumor Cells." *Journal of Virology* 71 (1): 715–19. https://doi.org/10.1128/jvi.71.1.715-
1029 719.1997.
1030 Stoecklin, Georg, Thomas Mayo, and Paul Anderson. 2006. "ARE-MRNA Degradation Requires
1031 the 5'-3' Decay Pathway." *EMBO Reports* 7 (1): 72–77.
1032 https://doi.org/10.1038/sj.embor.7400572.
1033 Sugimoto, Wataru, Katsuhiko Itoh, Yasumasa Mitsui, Takahiro Ebata, Hideaki Fujita, Hiroaki
1034 Hirata, and Keiko Kawauchi. 2018. "Substrate Rigidity-Dependent Positive Feedback
1035 Regulation between YAP and ROCK2." *Cell Adhesion and Migration* 12 (2): 101–8.
1036 https://doi.org/10.1080/19336918.2017.1338233.
1037 Takahashi, Shinya, Kyoko Sakurai, Arisa Ebihara, Hiroaki Kajiho, Kota Saito, Kenji Kontani,
1038 Hiroshi Nishina, and Toshiaki Katada. 2011. "RhoA Activation Participates in
1039 Rearrangement of Processing Bodies and Release of Nucleated AU-Rich MRNAs." *Nucleic*
1040 *Acids Research* 39 (8): 3446–57. https://doi.org/10.1093/nar/gkq1302.
1041 Tan, John L, Joe Tien, Dana M Pirone, Darren S Gray, Kiran Bhadriraju, and Christopher S
1042 Chen. 2003. "Cells Lying on a Bed of Microneedles: An Approach to Isolate Mechanical
1043 Force." *Proceedings of the National Academy of Sciences* 100 (4): 1484–89.
1044 https://doi.org/10.1073/pnas.0235407100.
1045 Tojkander, Sari, Gergana Gateva, and Pekka Lappalainen. 2012. "Actin Stress Fibers -
1046 Assembly, Dynamics and Biological Roles." *Journal of Cell Science* 125 (Pt 8): 1855–64.
1047 https://doi.org/10.1242/jcs.098087.
1048 Totaro, Antonio, Qiuyu Zhuang, Tito Panciera, Giusy Battilana, Luca Azzolin, Giulia Brumana,
1049 Alessandro Gandin, Giovanna Brusatin, Michelangelo Cordenonsi, and Stefano Piccolo.
1050 2019. "Cell Phenotypic Plasticity Requires Autophagic Flux Driven by YAP/TAZ
1051 Mechanotransduction." *Proceedings of the National Academy of Sciences* 116 (36): 17848–
1052 57. https://doi.org/10.1073/pnas.1908228116.
1053 Umbach, Jennifer L., Hui Ling Yen, Leo L M Poon, and Bryan R. Cullen. 2010. "Influenza a
1054 Virus Expresses High Levels of an Unusual Class of Small Viral Leader RNAs in Infected
1055 Cells." *MBio* 1 (4): 1–8. https://doi.org/10.1128/mBio.00204-10.
1056 Vallenius, Tea. 2013. "Actin Stress Fibre Subtypes in Mesenchymal-Migrating Cells." *Open*
1057 *Biology* 3 (6): 130001. https://doi.org/10.1098/rsob.130001.

1058 Vassilev, Alex, Kotaro J. Kaneko, Hongjun Shu, Yingming Zhao, and Melvin L. DePamphilis.
1059 2001. "TEAD/TEF Transcription Factors Utilize the Activation Domain of YAP65, a
1060 Src/Yes-Associated Protein Localized in the Cytoplasm." *Genes and Development* 15 (10):
1061 1229–41. https://doi.org/10.1101/gad.888601.
1062 Vindry, Caroline, Aline Marnef, Helen Broomhead, Laure Twyffels, Sevim Ozgur, Georg
1063 Stoecklin, Miriam Llorian, et al. 2017. "Dual RNA Processing Roles of Pat1b via
1064 Cytoplasmic Lsm1-7 and Nuclear Lsm2-8 Complexes." *Cell Reports* 20 (5): 1187–1200.
1065 https://doi.org/10.1016/j.celrep.2017.06.091.
1066 Vozzi, Federico, Jonica Campolo, Lorena Cozzi, Gianfranco Politano, Stefano Di Carlo, Michela
1067 Rial, Claudio Domenici, and Oberdan Parodi. 2018. "Computing of Low Shear Stress-
1068 Driven Endothelial Gene Network Involved in Early Stages of Atherosclerotic Process."
1069 *BioMed Research International* 2018 (September): 1–12.
1070 https://doi.org/10.1155/2018/5359830.
1071 Wada, K.-I., K. Itoga, T. Okano, S. Yonemura, and H. Sasaki. 2011. "Hippo Pathway Regulation
1072 by Cell Morphology and Stress Fibers." *Development* 138 (18): 3907–14.
1073 https://doi.org/10.1242/dev.070987.
1074 Wakatsuki, T, B Schwab, N Thompson, and EL Elson. 2001. "Effects of Cytochalasin D and
1075 Latrunculin B on Mechanical Properties of Cells." *Journal of Cell Science* 114 (5): 1025–
1076 36.
1077 Wang, Huanru, Liang Chang, Xiaohui Wang, Airong Su, Chunhong Feng, Yuxuan Fu, Deyan
1078 Chen, Nan Zheng, and Zhiwei Wu. 2016. "MOV10 Interacts with Enterovirus 71 Genomic
1079 5′UTR and Modulates Viral Replication." *Biochemical and Biophysical Research*
1080 *Communications* 479 (3): 571–77. https://doi.org/10.1016/j.bbrc.2016.09.112.
1081 Wang, Kuei-Chun, Yi-Ting Yeh, Phu Nguyen, Elaine Limqueco, Jocelyn Lopez, Satenick
1082 Thorossian, Kun-Liang Guan, Yi-Shuan J. Li, and Shu Chien. 2016. "Flow-Dependent
1083 YAP/TAZ Activities Regulate Endothelial Phenotypes and Atherosclerosis." *Proceedings*
1084 *of the National Academy of Sciences* 113 (41): 11525–30.
1085 https://doi.org/10.1073/pnas.1613121113.
1086 Wang, Xiaoli, Yingying Zhang, Tang Feng, Guanyue Su, Jia He, Wenbo Gao, Yang Shen, and
1087 Xiaoheng Liu. 2018. "Fluid Shear Stress Promotes Autophagy in Hepatocellular Carcinoma
1088 Cells." *International Journal of Biological Sciences* 14 (10): 1277–90.

1089 https://doi.org/10.7150/ijbs.27055.
1090 Watanabe, Naoki, Takayuki Kato, Akiko Fujita, Toshimasa Ishizaki, and Shuh Narumiya. 1999.
1091 "Cooperation between MDia1 and ROCK in Rho-Induced Actin Reorganization." *Nature*
1092 *Cell Biology* 1 (3): 136–43. https://doi.org/10.1038/11056.
1093 Watanabe, Naoki, Pascal Madaule, Tim Reid, Toshimasa Ishizaki, Go Watanabe, Akira
1094 Kakizuka, Yuji Saito, Kazuwa Nakao, Brigitte M. Jockusch, and Shuh Narumiya. 1997.
1095 "P140mDia, a Mammalian Homolog of Drosophila Diaphanous, Is a Target Protein for Rho
1096 Small GTPase and Is a Ligand for Profilin." *EMBO Journal* 16 (11): 3044–56.
1097 https://doi.org/10.1093/emboj/16.11.3044.
1098 Winzen, Reinhard, Michael Kracht, Birgit Ritter, Arno Wilhelm, Chyi Ying A. Chen, Ann Bin
1099 Shyu, Monika Müller, Matthias Gaestel, Klaus Resch, and Helmut Holtmann. 1999. "The
1100 P38 MAP Kinase Pathway Signals for Cytokine-Induced MRNA Stabilization via MAP
1101 Kinase-Activated Protein Kinase 2 and an AU-Rich Region-Targeted Mechanism." *EMBO*
1102 *Journal* 18 (18): 4969–80. https://doi.org/10.1093/emboj/18.18.4969.
1103 Yang, Chih-Sheng, Eleni Stampouloglou, Nathan M Kingston, Liye Zhang, Stefano Monti, and
1104 Xaralabos Varelas. 2018. "Glutamine-utilizing Transaminases Are a Metabolic
1105 Vulnerability of TAZ/YAP-activated Cancer Cells." *EMBO Reports* 19 (6): 1–11.
1106 https://doi.org/10.15252/embr.201643577.
1107 Yang, Ya Li, Lindsay M. Leone, and Laura J. Kaufman. 2009. "Elastic Moduli of Collagen Gels
1108 Can Be Predicted from Two-Dimensional Confocal Microscopy." *Biophysical Journal* 97
1109 (7): 2051–60. https://doi.org/10.1016/j.bpj.2009.07.035.
1110 Yao, Pingbo, Hong Zhao, Wenjuan Mo, and Pingping He. 2015. "Laminar Shear Stress
1111 Promotes Vascular Endothelial Cell Autophagy Through Upregulation with Rab4." *DNA*
1112 *and Cell Biology* 35 (3): 118–23. https://doi.org/10.1089/dna.2015.3041.
1113 Yu, Fa Xing, Bin Zhao, Nattapon Panupinthu, Jenna L. Jewell, Ian Lian, Lloyd H. Wang,
1114 Jiagang Zhao, et al. 2012. "Regulation of the Hippo-YAP Pathway by G-Protein-Coupled
1115 Receptor Signaling." *Cell* 150 (4): 780–91. https://doi.org/10.1016/j.cell.2012.06.037.
1116 Yu, Jiang Hong, Wei-Hong Yang, Tod Gulick, Kenneth D Bloch, and Donald B Bloch. 2005.
1117 "Ge-1 Is a Central Component of the Mammalian Cytoplasmic MRNA Processing Body."
1118 *RNA (New York, N.Y.)* 11 (12): 1795–1802. https://doi.org/10.1261/rna.2142405.
1119 Zanconato, Francesca, Mattia Forcato, Giusy Battilana, Luca Azzolin, Erika Quaranta, Beatrice

Bodega, Antonio Rosato, Silvio Bicciato, Michelangelo Cordenonsi, and Stefano Piccolo. 2015. "Genome-Wide Association between YAP/TAZ/TEAD and AP-1 at Enhancers Drives Oncogenic Growth." *Nature Cell Biology* 17 (9): 1218–27. https://doi.org/10.1038/ncb3216.

Zhang, Qian, Fansen Meng, Shasha Chen, Steven W Plouffe, Shiying Wu, Shengduo Liu, Xinran Li, et al. 2017. "Hippo Signalling Governs Cytosolic Nucleic Acid Sensing through YAP / TAZ-Mediated TBK1 Blockade." *Nature Cell Biology* 19 (4): 362–74. https://doi.org/10.1038/ncb3496.

Zhao, Bin, Li Li, Lloyd Wang, Cun Yu Wang, Jindan Yu, and Kun Liang Guan. 2012. "Cell Detachment Activates the Hippo Pathway via Cytoskeleton Reorganization to Induce Anoikis." *Genes and Development* 26 (1): 54–68. https://doi.org/10.1101/gad.173435.111.

Zhao, Bin, Bin Zhao, Xiaomu Wei, Xiaomu Wei, Weiquan Li, Weiquan Li, Ryan S Udan, et al. 2007. "Inactivation of YAP Oncoprotein by the Hippo Pathway Is Involved in Cell Contact Inhibition and Tissue Growth Control." *Genes and Development* 21: 2747–61. https://doi.org/10.1101/gad.1602907.Hpo/Sav.

Zhong, W, H Wang, B Herndier, and D Ganem. 1996. "Restricted Expression of Kaposi Sarcoma-Associated Herpesvirus (Human Herpesvirus 8) Genes in Kaposi Sarcoma." *Proceedings of the National Academy of Sciences of the United States of America* 93 (13): 6641–46. https://doi.org/10.1073/pnas.93.13.6641.

Acknowledgements

We would like to sincerely thank the members of the Corcoran lab for helpful discussions about this work, notably Carolyn-Ann Robinson. We would like to thank Dr. Craig McCormick (Dalhousie University) and his lab for plasmids, expertise and invaluable advice. ELC was supported by a Killam predoctoral scholarship, an NSERC CGS-M scholarship, and a Nova Scotia Graduate scholarship. Operating funds to support this work derive from an NSERC Discovery grant RGPIN-2015-04882 to JAC.

Competing Interests

The authors have no competing interests to declare.

Author Contributions

Elizabeth L. Castle: Conceptualization, Experimentation, Analysis, Paper Writing

Dr. Pauline Douglas: Experimentation

Dr. Kristina Rinker: Conceptualization

Dr. Jennifer A. Corcoran: Conceptualization, Experimentation, Supervision, Funding Acquisition, Project Administration, Paper Writing

Figures

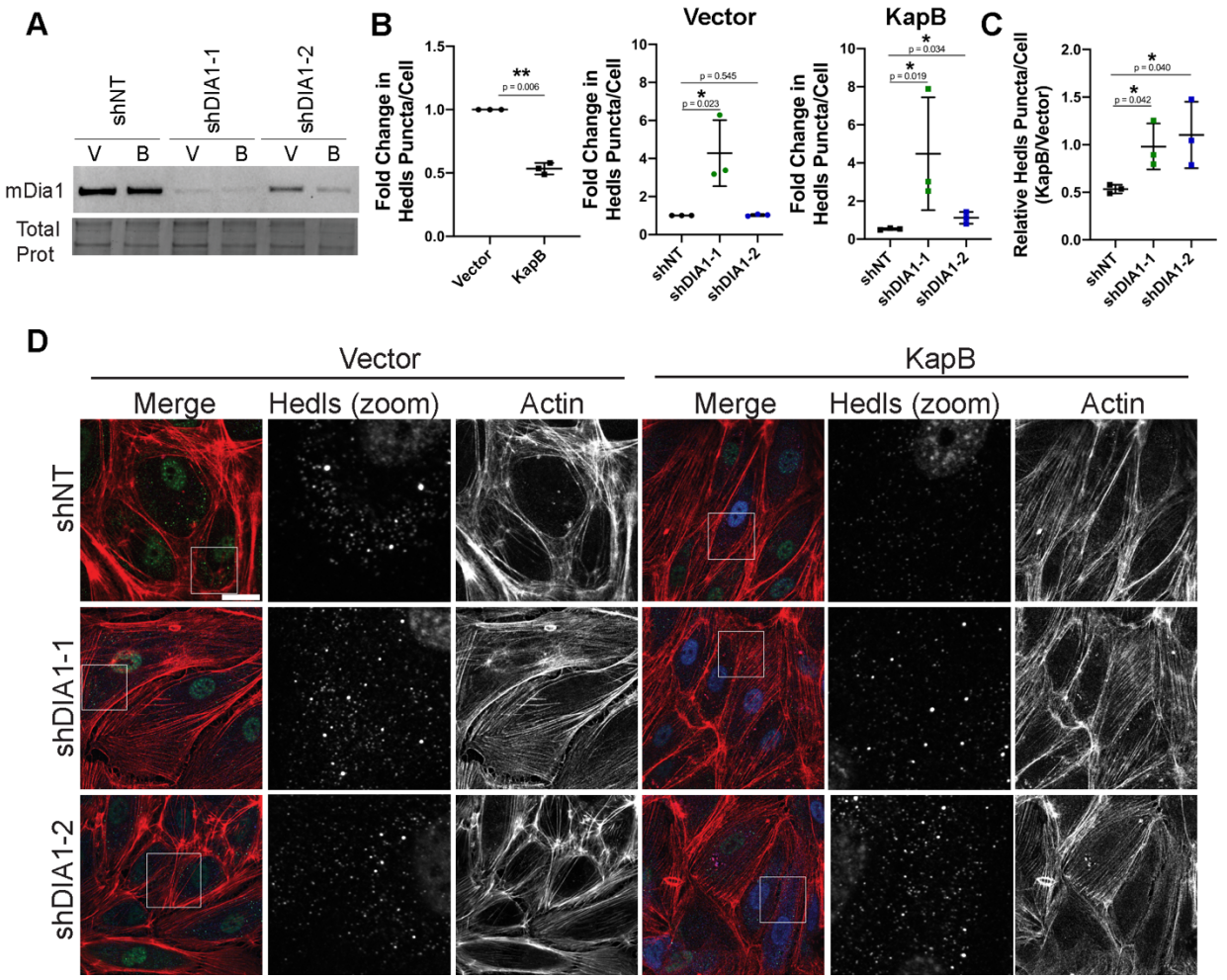

Figure 1: The RhoA-effector mDia1 is required for KapB-mediated PB disassembly. KapB- and vector- expressing HUVECs were transduced with shRNAs targeting mDia1 (shDIA1-1, shDIA1-2) or with a non-targeting (shNT) control and selected. In parallel, cells were fixed for immunofluorescence or lysed for immunoblotting. (A) One representative immunoblot of three independent experiments stained with mDia1-specific antibody is shown. (B, C) Fixed cells were stained for CellProfiler analysis as detailed in the methods. (B) The number of Hedls puncta per cell was quantified and normalized to the vector NT control within each replicate. (C) CellProfiler data was used to calculate the ratio of Hedls puncta counts in KapB-expressing cells versus the vector control for each treatment condition. (D) Representative images of cells stained for PB-resident protein Hedls (green), KapB (blue), and F-actin (red, phalloidin). Boxes indicate area shown in the Hedls (zoom) panel. Scale bar represents 20 μm. Statistics were determined using ratio paired t-tests between control and experimental groups; error bars represent standard deviation; n=3 independent biological replicates; * = $p < 0.05$, ** = $p < 0.01$.

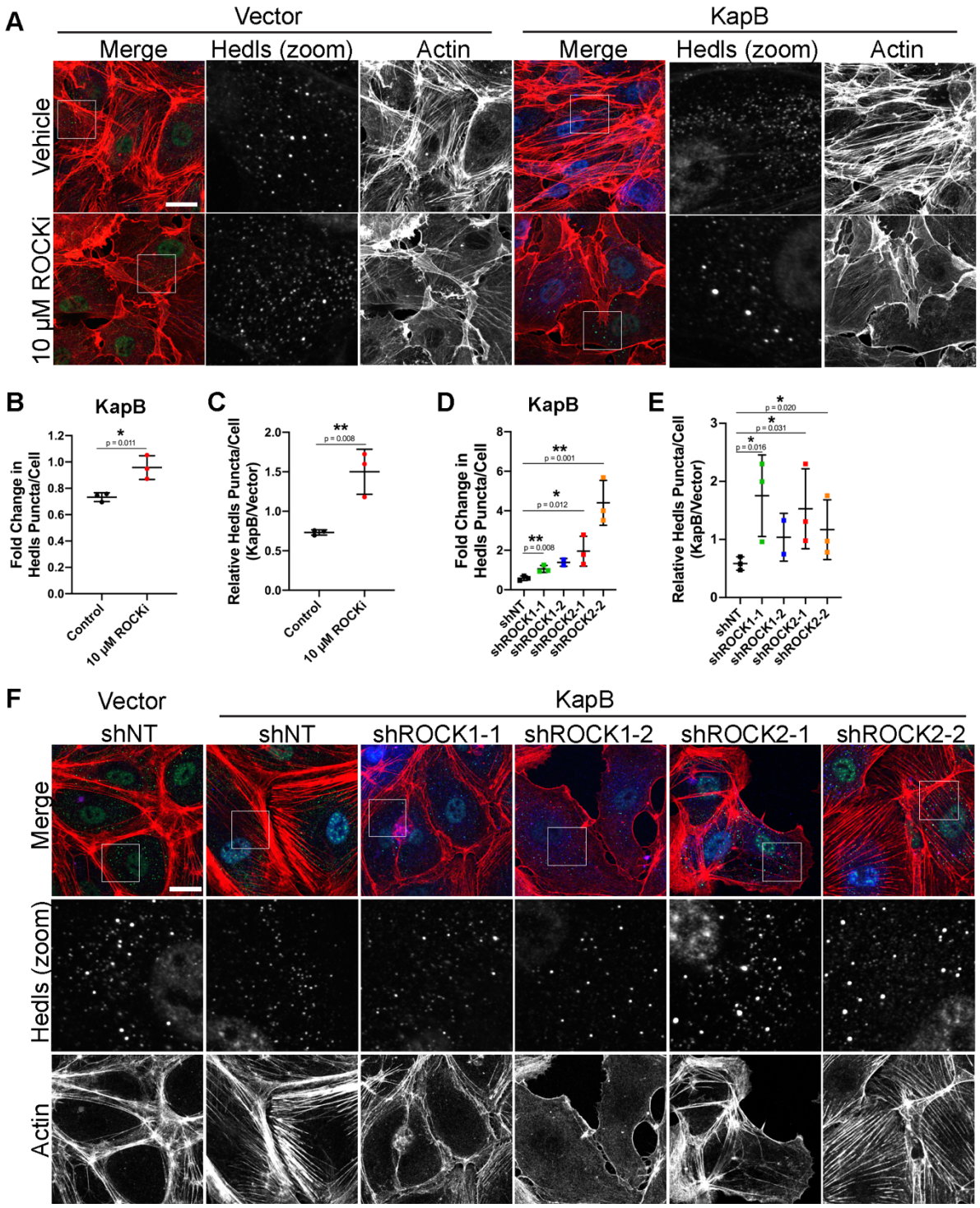

Figure 2: The RhoA-effector ROCK is required for KapB-mediated PB disassembly. (A-C) KapB- and vector- expressing HUVECs were treated with 10 ⌈M Y-27632 or water control for 4 h and fixed for immunofluorescence. (A) Representative images of cells stained for PB-resident protein Hedls (green), KapB (blue), and F-actin (red, phalloidin). Boxes indicate area shown in the Hedls (zoom) panel. Scale bar represents 20 μm. (B, C) Fixed cells were stained for CellProfiler analysis as detailed in the methods. (B) The number of Hedls puncta per cell was

1189 quantified and normalized to the vector NT control within each replicate. (C) CellProfiler data
1190 was used to calculate the ratio of Hedls puncta counts in KapB-expressing cells versus the vector
1191 control for each treatment condition. (D-F) KapB- and vector- expressing HUVECs were
1192 transduced with shRNAs targeting ROCK1 and ROCK2 (shROCK1-1, shROCK1-2, shROCK2-
1193 1, shROCK2-2) or with a non-targeting (shNT) control and selected. Cells were fixed for
1194 immunofluorescence. (D, E) Fixed cells were stained for CellProfiler analysis as detailed in the
1195 methods. (D) The number of Hedls puncta per cell was quantified and normalized to the vector
1196 NT control within each replicate. (E) CellProfiler data was used to calculate the ratio of Hedls
1197 puncta counts in KapB-expressing cells versus the vector control for each treatment condition.
1198 (F) Representative images of cells stained for PB-resident protein Hedls (green), KapB (blue),
1199 and F-actin (red, phalloidin). Boxes indicate images shown in Hedls (zoom) panel. Scale bar
1200 represents 20 μm. Statistics were determined using ratio paired t-tests between control and
1201 experimental groups; error bars represent standard deviation from n=3 independent biological
1202 replicates except shROCK1-2, (n=2); * = $p < 0.05$, ** = $p < 0.01$.
1203

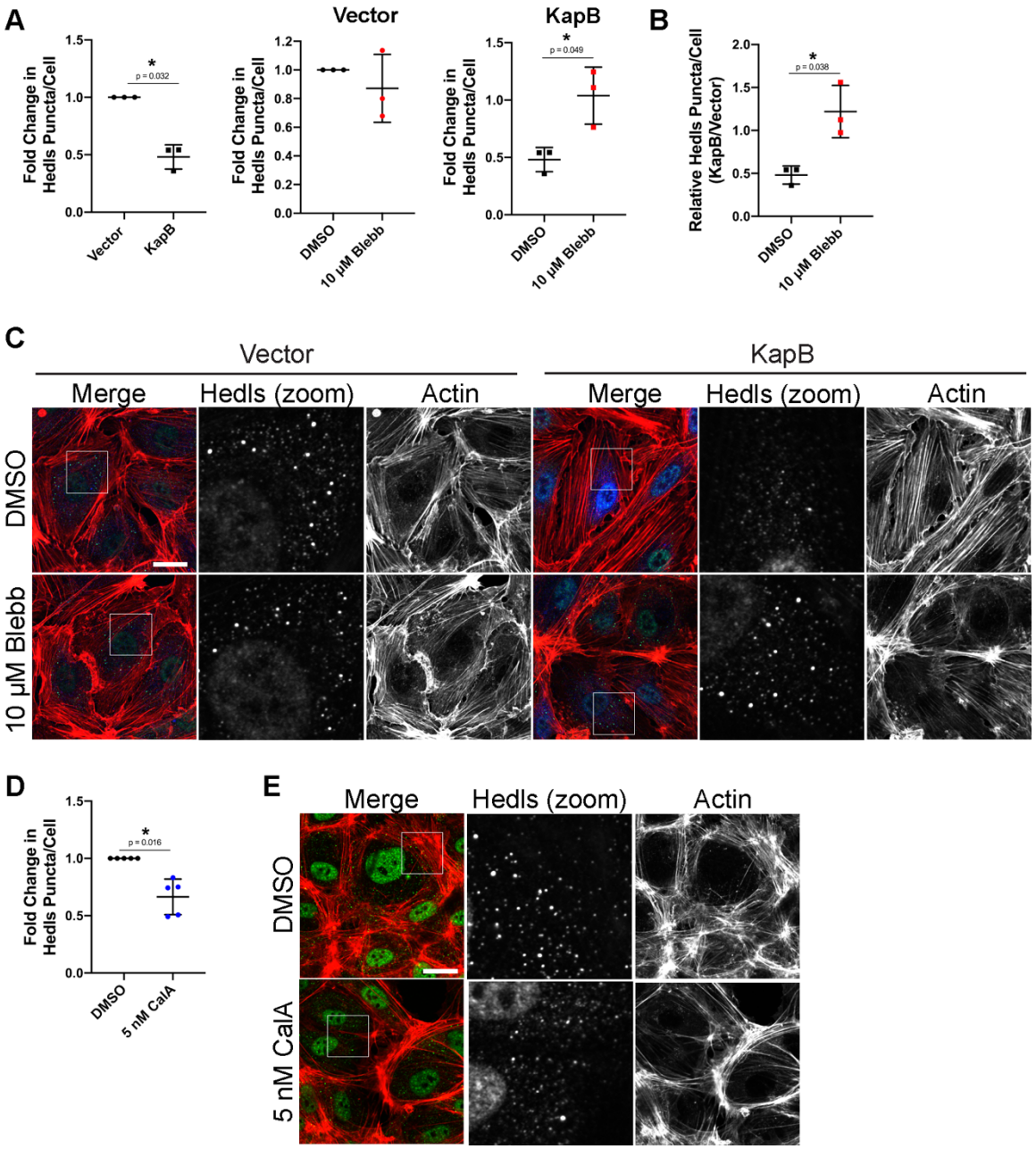

Figure 3: Actomyosin contractility controls PB disassembly. (A-C) KapB- and vector-expressing HUVECs were treated with 10 ⌈M blebbistatin to inhibit actomyosin contractility or DMSO for 30 min and fixed for immunofluorescence. (A, B) Fixed cells were stained for CellProfiler analysis as detailed in the methods. (A) The number of Hedls puncta per cell was quantified and normalized to the vector NT control within each replicate. (B) CellProfiler data was used to calculate the ratio of Hedls puncta counts in KapB-expressing cells versus the vector control for each treatment condition. (C) Representative images of cells stained for PB-resident protein Hedls (green), KapB (blue), and F-actin (red, phalloidin). Boxes indicate area shown in the Hedls (zoom) panel. Scale bar represents 20 μm. (D, E) Untransduced HUVECs were treated with 5 nM Calyculin A (CalA) to stimulate actomyosin contraction or DMSO for 20 min and fixed for immunofluorescence. (D) Fixed cells were stained for CellProfiler analysis as detailed

1217 in the methods. Hedls puncta per cell were quantified and normalized to the DMSO control
1218 within each replicate. (E) Representative images of cells treated with 5 nM CalA and stained for
1219 PB-resident protein Hedls (green) and F-actin (red, phalloidin). Boxes indicate area shown in the
1220 Hedls (zoom) panel. Scale bar represents 20 μm. Statistics were determined using ratio paired t-
1221 tests between control and experimental groups; error bars represent standard deviation; n=3 (A,
1222 B) and n=5 (D) independent biological replicates; * = $p < 0.05$.
1223
1224

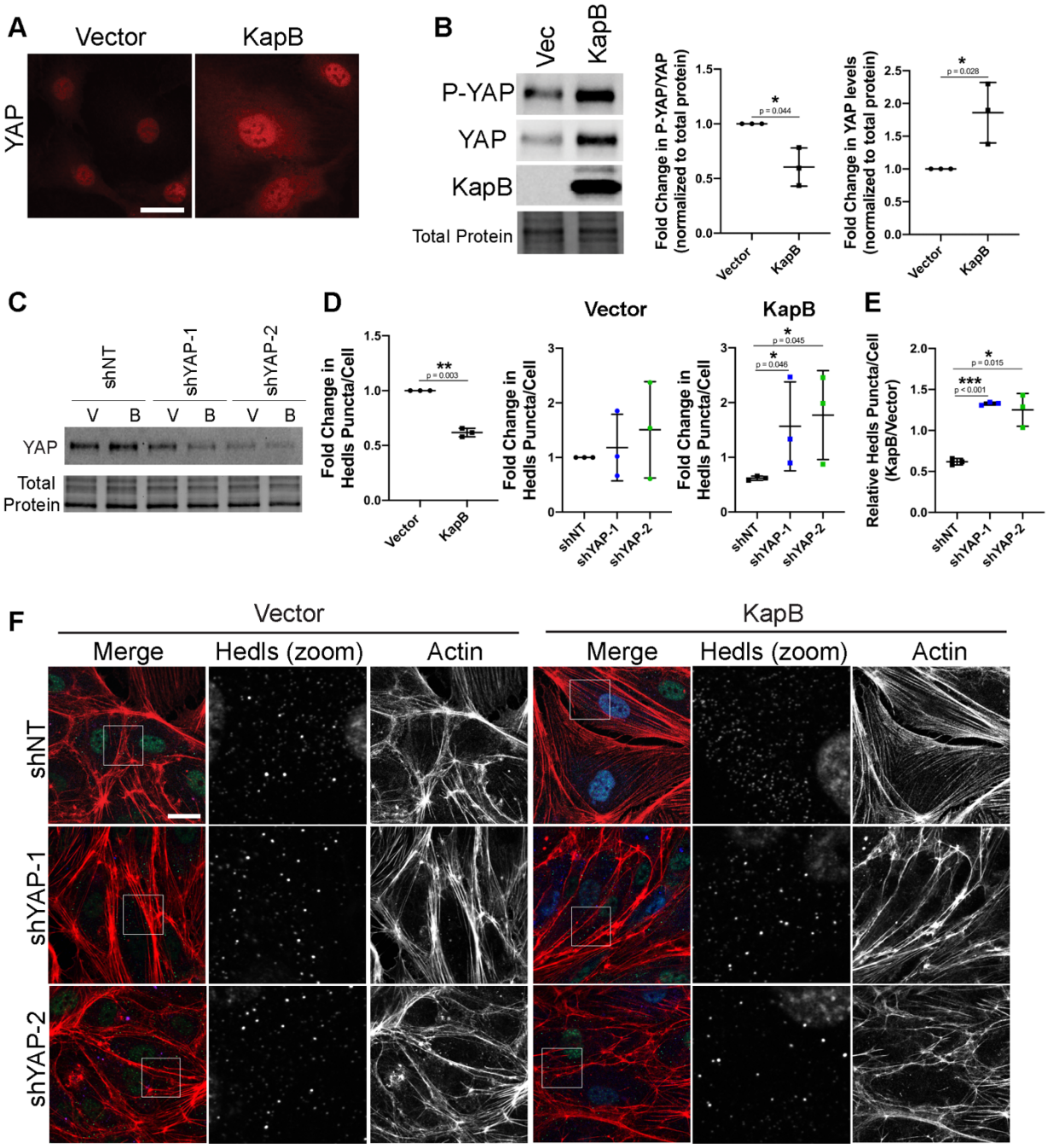

Figure 4: YAP is required for KapB-mediated PB disassembly. (A, B) KapB- and vector-expressing HUVECs were fixed for immunofluorescence or lysed for immunoblotting. (A) Representative images of cells stained for YAP (red). Scale bar represents 20 μM. (B) One representative immunoblot and quantification of three independent experiments stained with P(S127)-YAP-, YAP- or KapB-specific antibody are shown. Protein levels in each condition were normalized to total protein. All treatments were normalized to vector control within each replicate. (C-F) KapB- and vector- expressing HUVECs were transduced with shRNAs targeting YAP (shYAP-1, shYAP-2) or with a non-targeting (shNT) control and selected. In parallel, cells were fixed for immunofluorescence or lysed for immunoblotting. (C) One representative

1236 immunoblot of three independent experiments stained with YAP-specific antibody is shown. (D,
1237 E) Fixed cells were stained for CellProfiler analysis as detailed in the methods. (D) The number
1238 of Hedls puncta per cell was quantified and normalized to the vector NT control within each
1239 replicate. (E) CellProfiler data was used to calculate the ratio of Hedls puncta count in KapB-
1240 expressing cells to the vector control for each treatment condition. (F) Representative images of
1241 cells stained for PB-resident protein Hedls (green), KapB (blue), and F-actin (red, phalloidin).
1242 Boxes indicate area shown in the Hedls (zoom) panel. Scale bar represents 20 μm. Statistics were
1243 determined using ratio paired t-tests between control and experimental groups; error bars
1244 represent standard deviation; n=3 independent biological replicates; * = $p < 0.05$, ** = $p < 0.01$,
1245 *** = $p < 0.001$.
1246
1247

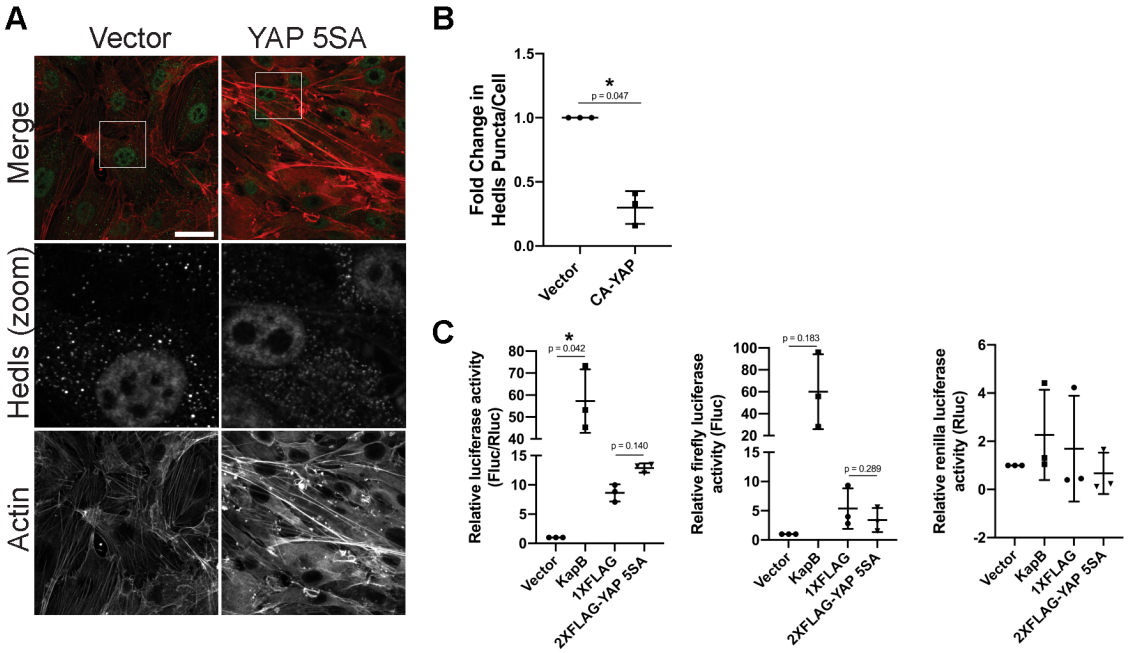

Figure 5: Active YAP elicits PB disassembly. (A, B) HUVECs were transduced with YAP 5SA-expressing and empty vector lentivirus and selected. Cells were fixed for immunofluorescence. (A) Representative images of cells stained for PB-resident protein Hedls (green) and F-actin (red, phalloidin). Boxes indicate area shown in the Hedls (zoom) panel. Scale bar represents 20 μm. (B) Fixed cells were stained for CellProfiler analysis as detailed in the methods. The number of Hedls puncta per cell was quantified and normalized to the vector control. (C) HeLa Tet-Off cells were seeded and co-transfected with an ARE-containing Firefly luciferase (Fluc) reporter plasmid, a Renilla luciferase (Rluc) reporter plasmid lacking an ARE, and either a KapB, YAP 5SA expression plasmid or vector controls. At 36 h post-transfection, transcription was terminated with doxycycline treatment for 12 h. Fluc and Rluc activity was measured. Data is normalized to vector control within each replicate. Graphs show the ratio of Fluc to Rluc, independent Fluc values and independent Rluc values, respectively. Statistics were determined using ratio paired t-tests between control and experimental groups (B) or repeated measures ANOVA (C); error bars represent standard deviation; n=3 independent biological replicates; * = $p < 0.05$, ** = $p < 0.01$.

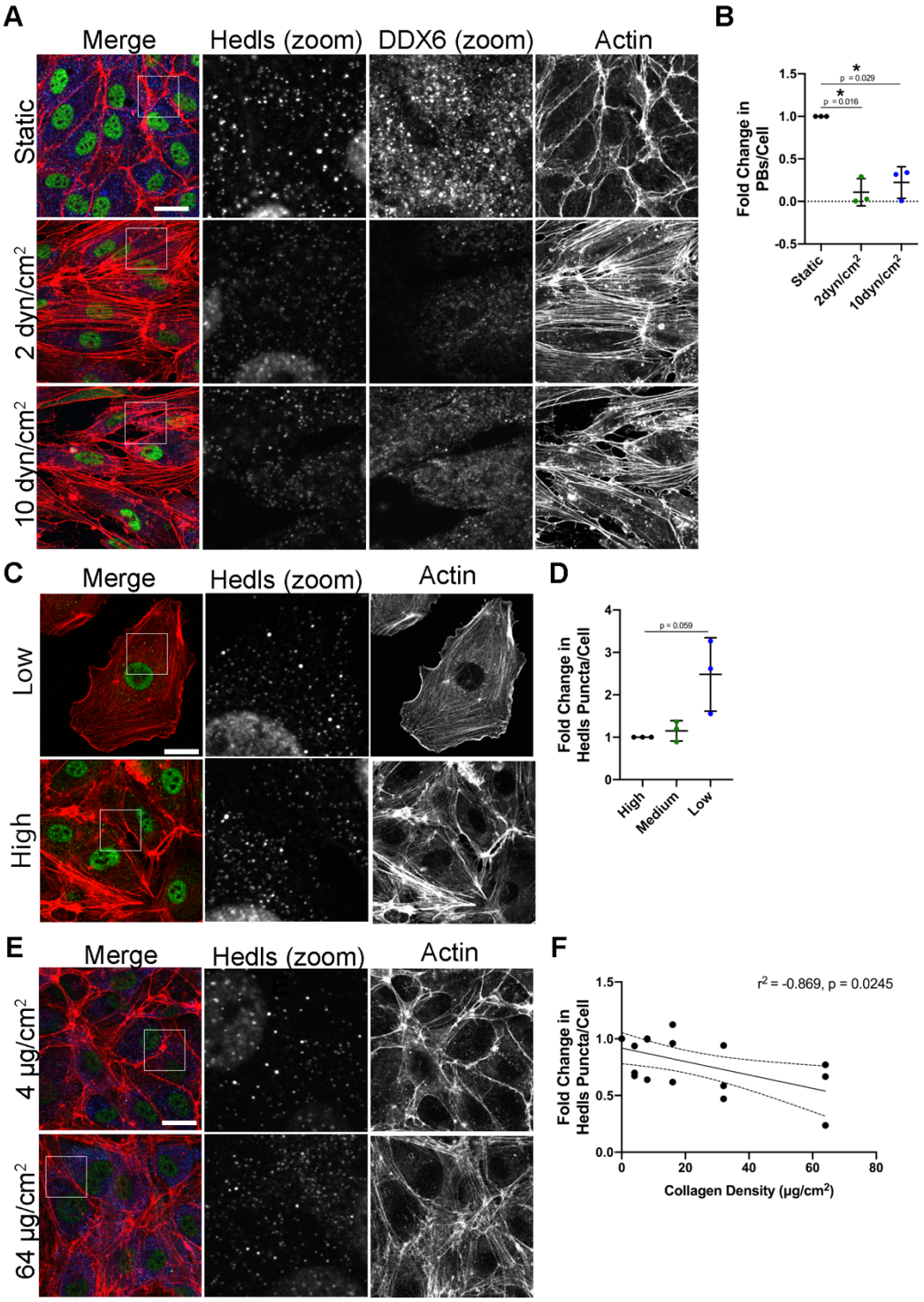

Figure 6: YAP Inputs Mediate PB Disassembly. (A, B) HUVECs were seeded onto collagen-coated microscope slides and exposed to shear stress of 2 dyn/cm^2, 10 dyn/cm^2 or no shear (static control) for 21 h. Cells were fixed and stained for immunofluorescence. (A) Representative images of cells stained for PB-resident proteins Hedls (green) and DDX6 (blue), as well as F-actin (red, phalloidin). Boxes indicate area shown in Hedls (zoom) and DDX6 (zoom) panels. Scale bar represents 20 μm. (B) CellProfiler was used to count nuclei, Hedls puncta and DDX6

puncta. In RStudio analysis, puncta with ≥ 70% correlation between Hedls and DDX6 (PBs) were counted and normalized to number of nuclei per condition. PB counts were normalized to static control within each replicate. (C, D) HUVECs were split and seeded at a high-, medium- and low-density, cultured for 48 h and fixed for immunofluorescence. (C) Representative images of cells stained for the PB-resident protein Hedls (green) and F-actin (red, phalloidin). Boxes indicate images shown in Hedls (zoom) panel. Scale bar represents 20 μm. (D) Fixed cells were stained for CellProfiler analysis as detailed in the methods. The number of Hedls puncta per cell was quantified and normalized to the high confluence condition. (E, F) Coverslips were coated for 4 h with 0 to 64 μg/cm^2 of collagen. HUVECs were grown for 72 h on coated coverslips and fixed for immunofluorescence. (E) Representative images of cells stained for PB-resident protein Hedls (green), DDX6 (blue) and F-actin (red, phalloidin). Boxes indicate images shown in Hedls (zoom) panel. Scale bar represents 20 μm. (F) Fixed cells were stained for CellProfiler analysis as detailed in the methods. The number of Hedls puncta per cell was quantified and normalized to the 0 μg/mL collagen-coating condition. Statistics were determined using repeated measures ANOVA (A, B) or Pearson's correlation co-efficient (C); error bars represent standard deviation (A, B) and 95% confidence interval of line of best fit (slope is significantly non-zero, $p = 0.014$) (C); n=3 independent biological replicates; * = $p < 0.05$, ** = $p < 0.01$.

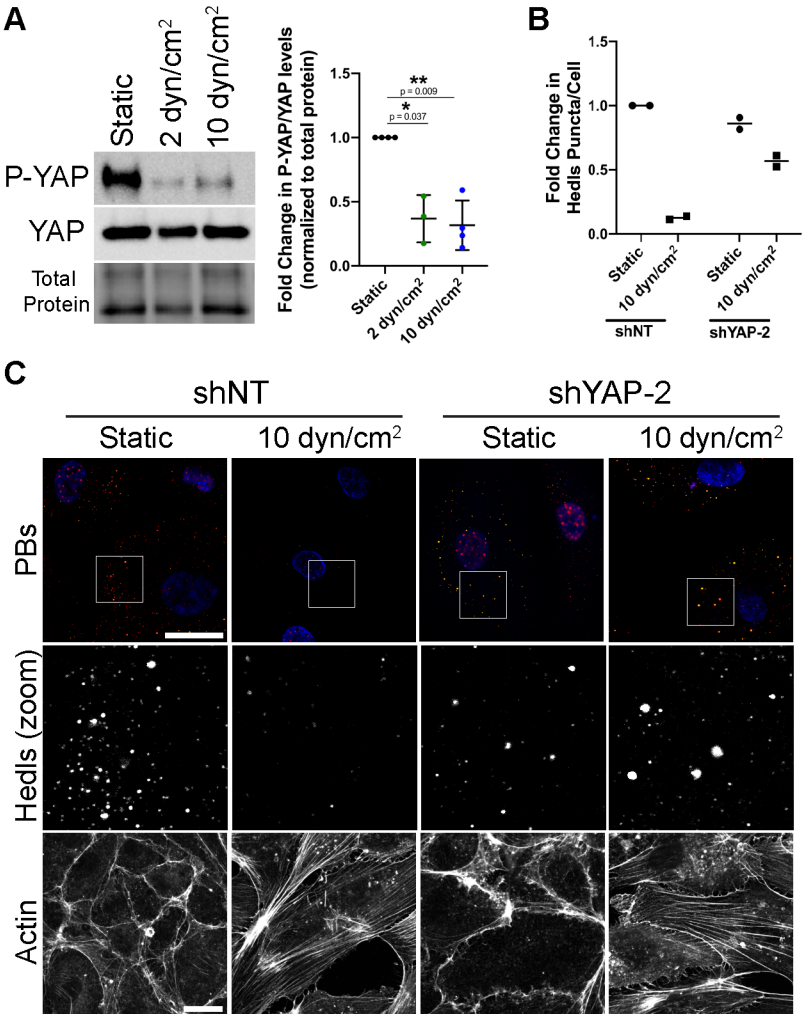

Figure 7: YAP is required for Hedls puncta disassembly in HUVECs subjected to shear stress. (A) HUVECs were seeded onto collagen-coated microscope slides and exposed to shear stress of 2 dyn/cm^2, 10 dyn/cm^2 or a static control for 21 h. Cells were lysed for immunoblotting. One representative immunoblot and quantification of three independent experiments stained with P(S127)-YAP- and YAP-specific antibody is shown. P(S127)-YAP and YAP protein levels in each condition were normalized to total protein. All treatments were normalized to static control within each replicate. (B, C) HUVECs were transduced with shRNAs targeting YAP (shYAP-2) or with a non-targeting (shNT) control and selected. Cells were seeded onto collagen-coated microscope slides and exposed to shear stress of 10 dyn/cm^2 or no shear (static control) for 21 h. Cells were fixed and stained for immunofluorescence. (B) CellProfiler was used to count nuclei and Hedls puncta. In RStudio analysis, Hedls puncta were normalized to number of nuclei per condition. Hedls puncta counts were normalized to static control. (C) Representative images of cells stained for PB-resident protein Hedls (red), DDX6 (green) and DAPI (blue). In parallel, separate coverslips were stained for F-actin (phalloidin). Boxes indicate area shown in the Hedls (zoom) panel. Scale bar represents 20 μm. Statistics were determined using repeated measures ANOVA (A); error bars represent standard deviation (A) ; n=4, except 2 dyn/cm^2 (n=3) (A) and n = 2 (B, C) independent biological replicates; * = $p < 0.05$, ** = $p < 0.01$.

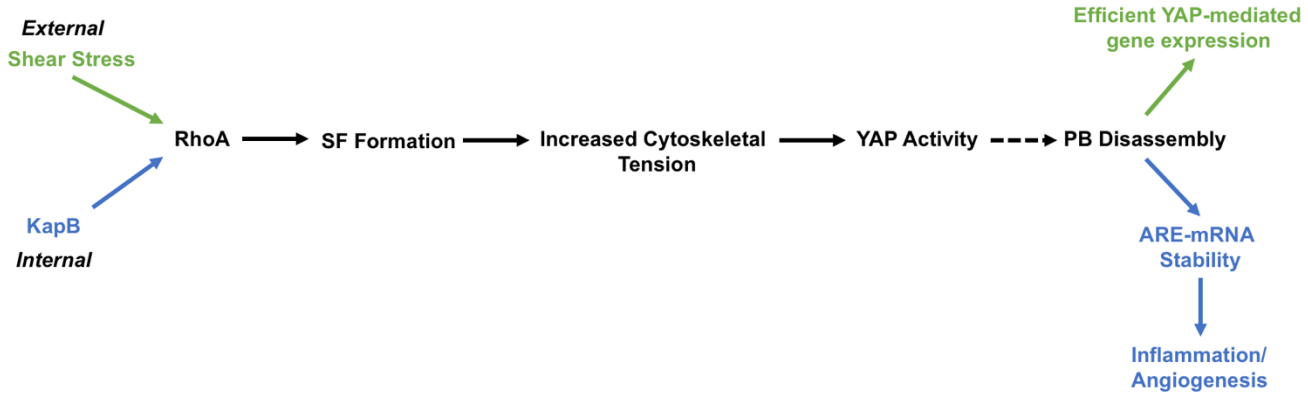

Figure 8: KapB activates a mechanoresponsive pathway from within the cell rather than without to mediate PB disassembly. Cells respond to external mechanical force by activating their structural support network, the actin cytoskeleton. The GTPase RhoA and its downstream effectors coordinate this response, bundling actin filaments into stress fibers (SFs), enhancing actomyosin contractility and increasing adhesion to the underlying matrix to help withstand force-induced membrane deformation. Together, these actin-based responses increase cytoskeletal tension and elicit the dephosphorylation and nuclear translocation of the mechanoresponsive transcription activator YAP where it collaborates with other transcription factors to induce TEAD-responsive genes. We present data to support the existence of a novel mechanoresponsive pathway that links actin SFs, actomyosin contractility, and the transcription transactivator YAP to the disassembly of PBs. The viral protein KapB taps into this mechanoresponsive pathway to trigger mechanical changes to cytoskeletal structures and downstream effectors that would normally respond to force, thereby inducing PB disassembly from within the cell, rather than from without.

1328 **Supplementary Information**

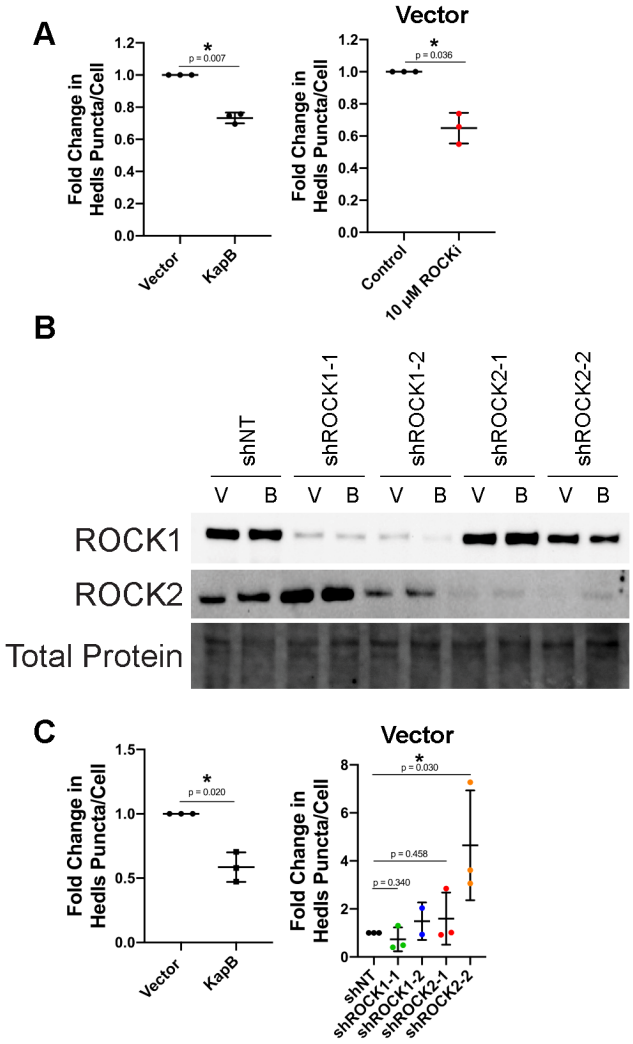

1329
1330
1331 **Figure S1: The RhoA-effector ROCK is required for KapB-mediated PB disassembly,**
1332 **knockdown confirmation and vector data.** (A) KapB- and vector- expressing HUVECs were
1333 treated with 10 μM Y-27632 or water control for 4 h and fixed for immunofluorescence. Fixed
1334 cells were stained for CellProfiler analysis as detailed in the methods. The number of Hedls
1335 puncta per cell was quantified and normalized to the vector control. Vector control data is
1336 shown. (B, C) KapB- and vector- expressing HUVECs were transduced with shRNAs targeting
1337 ROCK1 and ROCK2 (shROCK1-1, shROCK1-2, shROCK2-1, shROCK2-2) or with a non-
1338 targeting (shNT) control and selected. In parallel, cells were lysed for immunoblotting or fixed
1339 for immunofluorescence. (B) One representative immunoblot of three independent experiments
1340 stained using ROCK1- and 2-specific antibodies. (C) Fixed cells were stained for CellProfiler
1341 analysis as detailed in the methods. The number of Hedls puncta per cell was quantified and
1342 normalized to the vector NT control within each replicate. Vector control data is shown.
1343 Statistics were determined using a ratio paired t-test between control and experimental groups;
1344 error bars represent standard deviation; n=3 independent biological replicates; * = $p < 0.05$.
1345

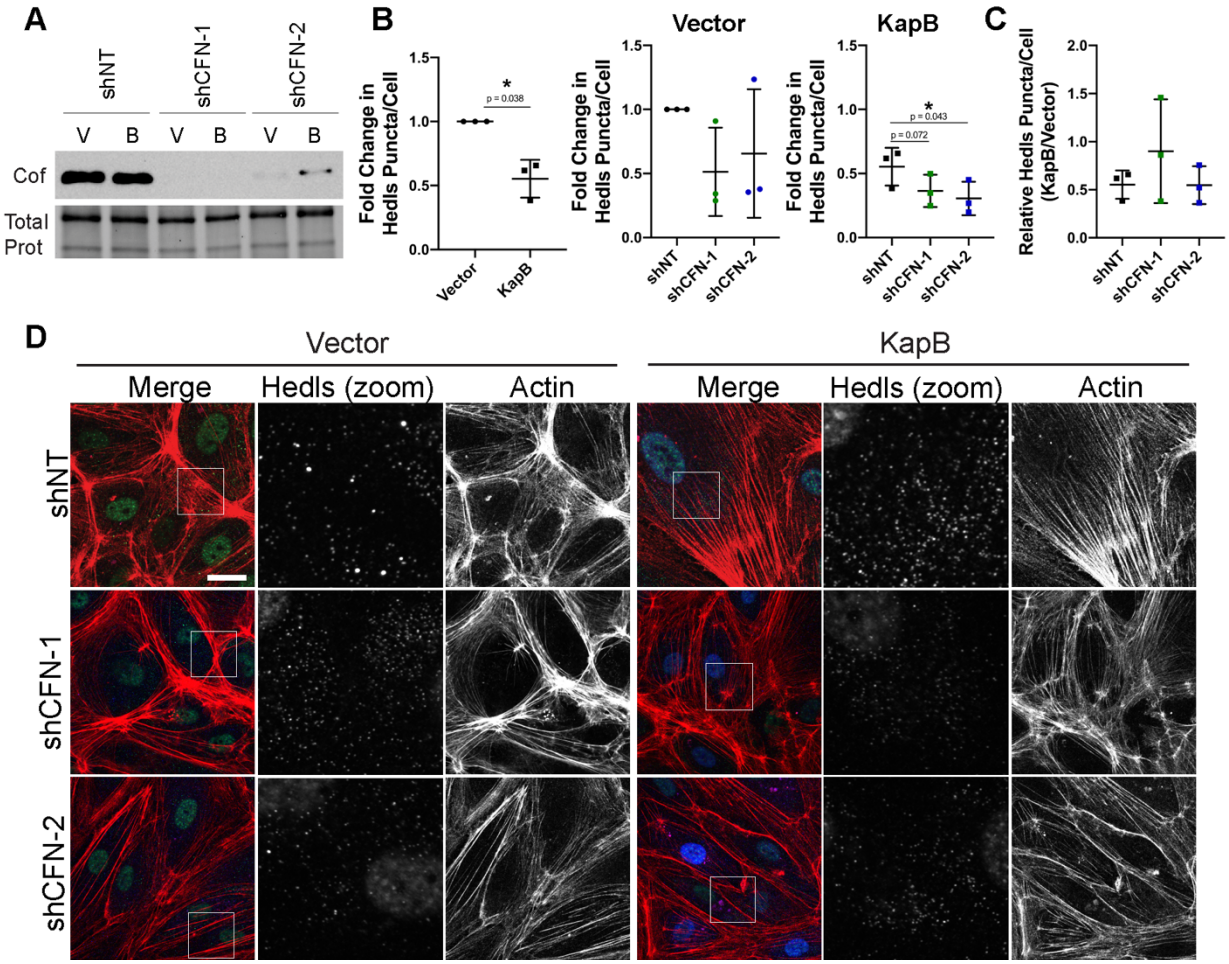

Figure S2: Cofilin knockdown augments KapB-mediated PB disassembly. KapB- and vector- expressing HUVECs were transduced with shRNAs targeting cofilin (shCFN-1, shCFN-2) or with a non-targeting (shNT) control and selected. In parallel, cells were fixed for immunofluorescence or lysed for immunoblotting. (A) One representative immunoblot of three independent experiments stained using a cofilin-specific antibody. (B, C) Fixed cells were stained for CellProfiler analysis as detailed in the methods. (B) The number of Hedls puncta per cell was quantified and normalized to the vector NT control within each replicate. (C) CellProfiler data was used to calculate the ratio of Hedls puncta counts in KapB-expressing cells versus the vector control for each treatment condition. (D) Representative images of cells stained for PB-resident protein Hedls (green), KapB (blue), and F-actin (red, phalloidin). Boxes indicate the area of the field of view that is shown in Hedls (zoom) panel. Scale bar represents 20 μm. Statistics were determined using a ratio paired t-test between control and experimental groups; error bars represent standard deviation; n=3 independent biological replicates; * = $p < 0.05$.

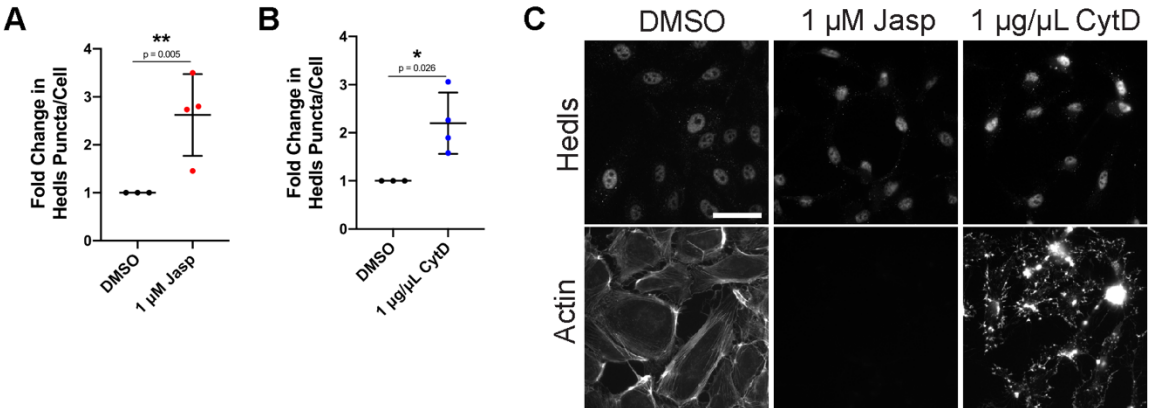

Figure S3: G-actin concentration does not control PB disassembly. (A, B, C) HUVECs were treated with 1 μM Jasp (polymerizes actin and decreases monomeric G-actin), 1 μg/μL CytD (actin depolymerization to increase monomeric G-actin) or a DMSO control for 30 min. (A, B) Fixed cells were stained for CellProfiler analysis as detailed in the methods. The number of Hedls puncta per cell was quantified and normalized to the DMSO control. (C) Representative images of cells stained for PB-resident protein Hedls and F-actin (phalloidin). Actin is not seen in Jasp panel due to Jasp-mediated interference with phalloidin staining (Bubb et al. 1999). Scale bar represents 20 μm. Statistics were determined using a ratio paired t-test between control and experimental groups; error bars represent standard deviation; n=3 independent biological replicates; * = $p < 0.05$, ** = $p < 0.01$.

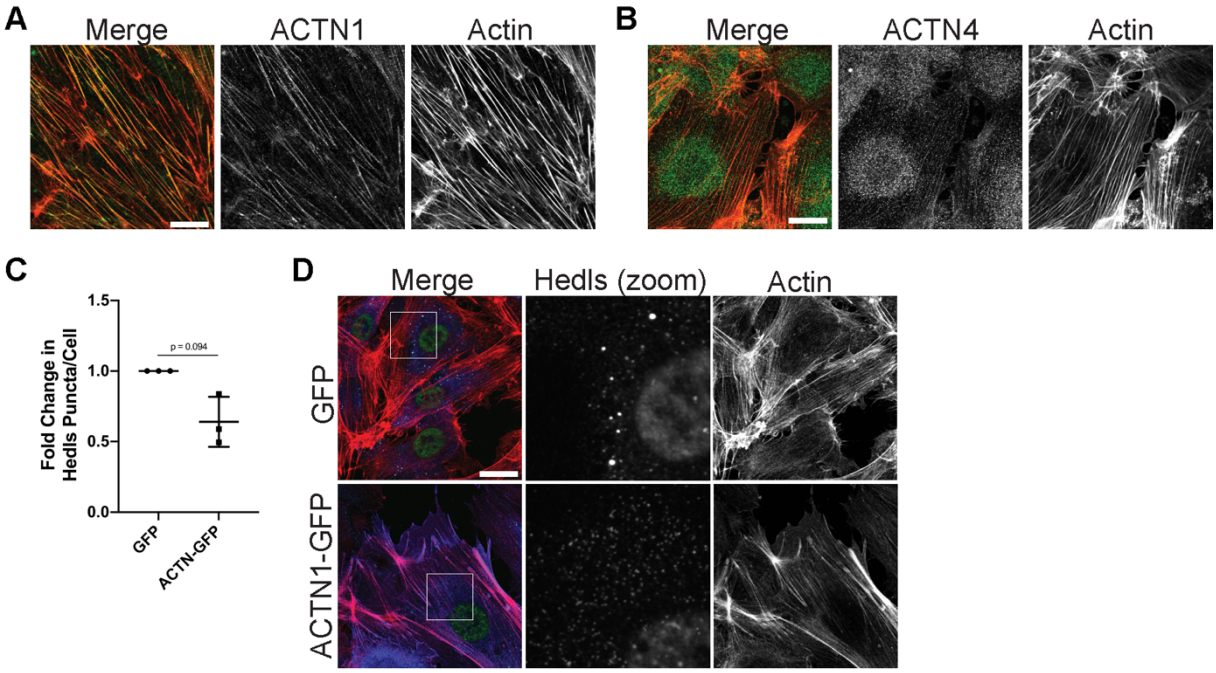

Figure S4: α-actinin-1-overexpression mediated SF formation and PB disassembly. HUVECs were fixed and stained with antibodies for (A) α-actinin-1 and (B) α-actinin-4. (C, D) HUVECs transduced with recombinant lentiviruses expressing GFP-tagged α-actinin-1 (ACTN-GFP) or a GFP control were selected and fixed for immunofluorescence. (C) Fixed cells were stained for CellProfiler analysis as detailed in the methods. The number of Hedls puncta per cell was quantified and normalized to the vector GFP control. (D) Representative images of cells stained for PB-resident protein Hedls (false-coloured green), ACTN-GFP (false-coloured blue), and F-actin (red, phalloidin). Boxes indicate images shown in Hedls (zoom) panel. Scale bar represents 20 μm. Statistics were determined using a ratio paired t-test between control and experimental groups; error bars represent standard deviation; n=3 independent biological replicates; * = $p < 0.05$.

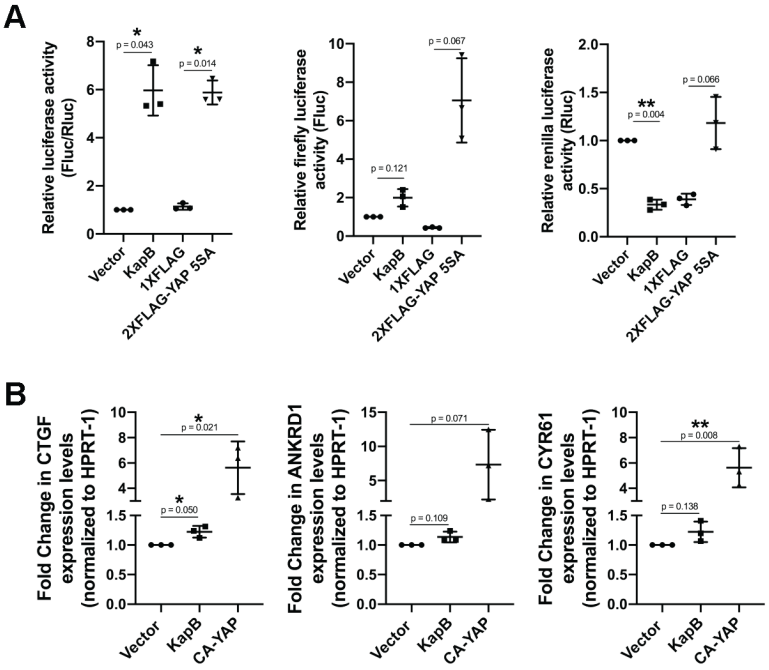

Figure S5: KapB does not induce transcription of canonical YAP-responsive genes. (A) HEK-293A cells were co-transfected with a firefly luciferase (Fluc) reporter plasmid with a YAP-responsive TEAD promoter element, a TREX-renilla luciferase (Rluc) reporter plasmid, and overexpression constructs for either a KapB, YAP 5SA or vector control. At 36 h post-transfection, cells were starved in serum-free DMEM for 12 h, lysed and Fluc and Rluc activity was recorded. Data is normalized to vector control. Graphs show the ratio of Fluc to Rluc, independent Fluc values and independent Rluc values, respectively. (B) HUVECs were transduced with recombinant lentiviruses expressing KapB, a constitutively-active version of YAP (YAP 5SA) or an empty vector control, selected and lysed for total RNA. qRT-PCR analysis of steady state mRNA levels of canonical YAP-regulated genes CTGF, ANKRD1 and CYR61 was performed, and was normalized to steady state HPRT-1 mRNA levels. Statistics were determined using repeated measures ANOVA; error bars represent standard deviation; n=3 independent biological replicates; * = $p < 0.05$, ** = $p < 0.01$.

1419 **Table S1: Antibodies used in this study.**

Antibody	Source	Use	Dilution
Rabbit ⟨-mDia1	Cell Signalling Technologies (Cat#:5486)	Immunoblotting	1:1000 in 2.5% BSA
Rabbit ⟨-ROCK1	Cell Signalling Technologies (Cat#:4035)	Immunoblotting	1:1000 in 2.5% BSA
Rabbit ⟨-ROCK2	Cell Signalling Technologies (Cat#:9029)	Immunoblotting	1:500 in 2.5% BSA
Rabbit ⟨-Cofilin	Cell Signalling Technologies (Cat#:5175)	Immunoblotting	1:1000 in 2.5% BSA
Rabbit ⟨-P-YAP	Cell Signalling Technologies (Cat#: 4911)	Immunoblotting	1:1000 in 2.5% BSA
Rabbit ⟨-YAP	Cell Signalling Technologies (Cat#: 4912)	Immunoblotting	1:1000 in 2.5% BSA
⟨-Mouse IgG, HRP-linked (2˚)	Cell Signalling Technologies (Cat#: 7076)	Immunoblotting	1:2000 to 1:4000 in 2.5% BSA
⟨-Rabbit IgG, HRP-linked (2˚)	Cell Signalling Technologies (Cat#: 7074)	Immunoblotting	1:2000 to 1:4000 in 2.5% BSA

Mouse ⟨-p70 s6 kinase (detects Hedls)	Santa Cruz (Cat#:sc-8418)	Immunofluorescence	1:1000 in blocking buffer (1% Human AB in PBS), 4˚C overnight
Rabbit ⟨-KapB	Gift from D. Ganem and C. McCormick	Immunofluorescence/ Immunoblotting	1:1000 in blocking buffer (1% Human AB in PBS), 30 min RT
Rabbit ⟨-actinin-1	Abclonal (Cat#:A1160)	Immunofluorescence	1:500 in blocking buffer (1% Human AB in PBS), 4˚C overnight
Mouse ⟨-actinin-4	Santa Cruz (Cat#:sc-390205)	Immunofluorescence	1:500 in blocking buffer (1% Human AB in PBS), 4˚C overnight
Mouse ⟨-YAP	Santa Cruz (Cat#:sc-101199)	Immunofluorescence	1:1000 in blocking buffer (1% Human AB in PBS), 4˚C overnight
Rabbit ⟨-DDX6	Bethyl Labs (Cat#:A300-461A)	Immunofluorescence	1:1000 in blocking buffer (1% Human AB in PBS), 4˚C overnight
Alexa Fluor 555-conjugated donkey ⟨-mouse IgG (2˚)	Invitrogen (Cat#:A31570)	Immunofluorescence	1:1000 in blocking buffer (1% Human AB in PBS), 1h RT
Alexa Fluor 488-conjugated chicken ⟨-rabbit IgG (2˚)	Invitrogen (Cat#:A21441)	Immunofluorescence	1:1000 in blocking buffer (1% Human AB in PBS), 1h RT
Alexa Fluor 555-conjugated donkey ⟨-rabbit IgG (2˚)	Invitrogen (Cat#:A31572)	Immunofluorescence	1:1000 in blocking buffer (1% Human AB in PBS), 1h RT
Alexa Fluor 488-conjugated chicken ⟨-mouse IgG (2˚)	Invitrogen (Cat#:A21200)	Immunofluorescence	1:1000 in blocking buffer (1% Human AB in PBS), 1h RT

1420
1421
1422

1423 **Table S2: Plasmids used in this study.**

Plasmid Name	Use	Source	Bacterial Selection Cassette	Mammalian Selection Cassette (Lentiviral Plasmids Only)
pLJM-1-EV	Control vector for lentiviral expression studies	C. McCormick (Dalhousie University)	Ampicillin	Blasticidin, Puromycin
pLJM-1 KapB	Lentiviral expression of KapB	C. McCormick (Dalhousie University)	Ampicillin	Blasticidin
pLKO-(shRNA)	Lentiviral expression of short hairpin RNAs (shRNA sequences in Table S3)	Cloned from: pLKO-TRC Addgene no.: 26655	Ampicillin	Puromycin
pLJM-1 ⟨-actinin1-GFP	Lentiviral expression of ⟨-actinin1-GFP	Cloned from: pEGFP-N1 ⟨-actinin-1, Addgene no.: 11908	Ampicillin	Puromycin
pLJM-1-YAP-5SA (CA-YAP)	Lentiviral expression of constitutively active YAP	Cloned from: p2XFLAG-YAP-5SA, Donated by C. McCormick (Dalhousie University)	Ampicillin	Blasticidin
pcDNA3.1	Transfection control	Invitrogen	Ampicillin	N/A
pcDNA3.1 KapB	Transfection of KapB	C. McCormick (Dalhousie University)	Ampicillin	N/A

p1XFLAG	Transfection control	Cloned from: p2XFLAG-YAP-5SA, Donated by C. McCormick (Dalhousie University)	Ampicillin	N/A
p2XFLAG-YAP 5SA	Transfection of YAP 5SA	Donated by C. McCormick (Dalhousie University)	Ampicillin	N/A
pMD2.G	Envelope protein for lentiviral production	Addgene no.: 12259	Ampicillin	N/A
psPAX2	Packaging proteins for lentiviral production	Addgene no.: 12260	Ampicillin	N/A

1424
1425
1426
1427

1428 **Table S3: shRNA sequences used in this study.**

Target	Sequence (5' – 3')
Non-targeting sense	CCGGAGCACAAGCTGGAGTACAACTACTCGAGATCAACATGAGGTCGAACACGATTTG
Non-targeting antisense	AATTCAAAAAGCACAAGCTGGAGTACAACTAATCAACATGAGGTCGAACACGATTTG
mDia1 sh1 sense	CCGGCCAATTCTGCTCATAGAAATTCTCGAGAATTTCTATGAGCAGAATTGGTTTTTG
mDia1 sh1 antisense	AATTCAAAAACCAATTCTGCTCATAGAAATTCTCGAGAATTTCTATGAGCAGAATTGG
mDia1 sh2 sense	CCGGAAGATGACGTTGTTACACTTCCTCGAGGAAGTGTAACAACGTCATCTTTTTTTG
mDia1 sh2 antisense	AATTCAAAAAAAGATGACGTTGTTACACTTCCTCGAGGAAGTGTAACAACGTCATCTT
ROCK1 sh1 sense	CCGGAAGATGACGTTGTTACACTTCCTCGAGGAAGTGTAACAACGTCATCTTTTTTTG
ROCK1 sh1 antisense	AATTCAAAAAAAGATGACGTTGTTACACTTCCTCGAGGAAGTGTAACAACGTCATCTT
ROCK1 sh2 sense	CCGGAAGATGACGTTGTTACACTTCCTCGAGGAAGTGTAACAACGTCATCTTTTTTTG
ROCK1 sh2 antisense	AATTCAAAAAAAGATGACGTTGTTACACTTCCTCGAGGAAGTGTAACAACGTCATCTT
ROCK2 sh1 sense	CCGGCGTTGCCATATTAAGTGTCATCTCGAGATGACACTTAATATGGCAACGTTTTTG
ROCK2 sh1 antisense	AATTCAAAAACGTTGCCATATTAAGTGTCATCTCGAGATGACACTTAATATGGCAACG
ROCK2 sh2 sense	CCGGGCCTTGCATATTGGTCTGGATCTCGAGATCCAGACCAATATGCAAGGCTTTTTG
ROCK2 sh2 antisense	AATTCAAAAAGCCTTGCATATTGGTCTGGATCTCGAGATCCAGACCAATATGCAAGGC

Cofilin sh1 sense	CCGGACGACATGAAGGTGCGTAAGTCTCGAGACTTACGCACCTTCATGTCGTTTTTTG
Cofilin sh1 antisense	AATTCAAAAAACGACATGAAGGTGCGTAAGTCTCGAGACTTACGCACCTTCATGTCGT
Cofilin sh2 sense	CCGGCCAGATAAGGACTGCCGCTATCTCGAGATAGCGGCAGTCCTTATCTGGTTTTTG
Cofilin sh2 antisense	AATTCAAAAACCAGATAAGGACTGCCGCTATCTCGAGATAGCGGCAGTCCTTATCTGG
YAP sh1 sense	CCGGCTGGTCAGAGATACTTCTTAACTCGAGTTAAGAAGTATCTCTGACCAGTTTTTC
YAP sh1 antisense	AATTGAAAAACTGGTCAGAGATACTTCTTAACTCGAGTTAAGAAGTATCTCTGACCAG
YAP sh2 sense	CCGGAAGCTTTGAGTTCTGACATCCCTCGAGGGATGTCAGAACTCAAAGCTTTTTTTC
YAP sh2 antisense	AATTGAAAAAAAGCTTTGAGTTCTGACATCCCTCGAGGGATGTCAGAACTCAAAGCTT

1432 **Table S4: Drug treatments used in this study.**

Drug	Use	Source (Cat#)	Concentration Used	Duration
Y-27623 dihydrochloride (ROCKi)	Non-isoform specific inhibition of ROCK	Sigma-Aldrich (Cat#:Y0503)	10 μM	4 h
Jasplakinolide	Aberrant polymerization of actin, decreasing monomeric G-actin	Sigma-Aldrich (Cat#:J4580)	0.5 μM, 1 μM	30 min
Cytochalasin D	Inhibition of actin polymerization, increasing monomeric G-actin	Sigma-Aldrich (C8273)	1 μg/mL	30 min
(-)-Blebbistatin	Inhibition of MLC contractility	Sigma-Aldrich (Cat#:B0560)	10 μM	30 min
Calyculin A	Inhibition of MLC phosphatase, resulting in cell contraction	Abcam (Cat#: ab141784)	2.5 nM, 5 nM	20 min

1433

1434

1435 **Table S5: qRT-PCR primers used in this study.**

Target	Forward/ Reverse	Sequence	Tm (˚C)	Reference
CYR61	Forward	ATGGTCCCAGTGCTCAAAGA	60	(K.-C. Wang et al. 2016)
CYR61	Reverse	GGGCCGGTATTTCTTCACAC	62	(K.-C. Wang et al. 2016)
CTGF	Forward	CAGCATGGACGTTCGTCTG	60	(K.-C. Wang et al. 2016)
CTGF	Reverse	AACCACGGTTTGGTCCTTGG	62	(K.-C. Wang et al. 2016)
CTGF	Forward	CCCTCGCGGCTTACCG	56	(K.-C. Wang et al. 2016)
CTGF	Reverse	GGACCAGGCAGTTGGCTCT	62	(K.-C. Wang et al. 2016)
ANKRD1	Forward	ACGCCAAAGACAGAGAAGGA	60	(K.-C. Wang et al. 2016)
ANKRD1	Reverse	TTCTGCCAGTGTAGCACCAG	52	(K.-C. Wang et al. 2016)
HPRT-1	Forward	CTTTCCTTGGTCAGGCAGTATAA	66	(Singh, 2019)
HPRT-1	Reverse	AGTCTGGCTTATATCCAACACTTC	60	(Singh, 2019)
HPRT-1	Forward	TGGCGTCGTGATTAGTGATG	64	(Singh, 2019)
HPRT-1	Reverse	GACGTTCAGTCCTGTCCATAAT	68	(Singh, 2019)

1436